Neural Computing and Applications (2024) 36:13665–13687
https://doi.org/10.1007/s00521-024-09791-y

ORIGINAL ARTICLE

PINN-CHK: physics-informed neural network for high-fidelity prediction of early-age cement hydration kinetics

Md Asif Rahman[1] · Tianjie Zhang[1] · Yang Lu[2]

Received: 14 October 2023 / Accepted: 25 March 2024 / Published online: 26 April 2024

Abstract
Cement hydration kinetics, characterized by heat generation in early-age concrete, poses a modeling challenge. This work proposes a physics-informed neural network (PINN) named PINN-CHK designed for cement hydration kinetics, to predict early-age temperature rises in cement paste. PINN-CHK leverages data-driven solutions to craft a high-fidelity prediction model, encompassing material properties and maturity functions in cement hydration. Trained on heated cement paste data, it simultaneously fits experimental results and underlying physics, yielding a mesh-free simulation. Incorporating governing partial differential equations (PDEs), and initial and boundary conditions into its loss function, PINN-CHK architecture undergoes rigorous benchmark testing, demonstrating unparalleled predictive accuracy compared to conventional deep-learning methods. It excels in predicting complete temperature fields during spatial–temporal cement hydration, achieving a remarkable relative L2 error as low as 0.00341. PINN-CHK achieves exceptional convergence and accuracy with only 5% of the training data, ushering in a new era in this crucial field. This innovative approach bridges the gap between theory and practice, offering an attractive alternative to conventional finite element solvers for enhanced comprehension of cement hydration kinetics and concrete maturity and strength development in cement-based materials.

Keywords Physics-informed neural network · Deep learning · Cement hydration kinetics · Hydration temperature · Cement-based materials

1 Introduction

Cement hydration is a chemical reaction between cement and water, resulting in the formation of calcium silicate hydrate (CSH) and calcium hydroxide (CH) in fresh concrete. This reaction involves two distinct types of water in the cement paste: evaporable and non-evaporable fractions, with the latter, known as chemically bound water, actively participating in the reaction [1]. CSH acts as the main binder, contributing to concrete strength, while CH provides early strength. The microstructure, characterized by a CSH network, is crucial for concrete properties. Optimization of hydration and consideration of curing conditions like initial curing temperature enhance concrete performance in applications.

The process of cement hydration is an exothermic reaction, resulting in the generation of heat and temperature rise within the cement paste [1]. This temperature rise is a critical factor in assessing the hydration process, where the concept of maturity is introduced to quantify the level of hydration progress [2]. This concept is intimately linked to temperature's influence on the rate of heat release, resulting in the development of an equivalent age concept [2]. Thus, intricate nonlinear physical interactions characterize the kinetics of cement hydration. Initially, the reaction generates heat rapidly, but the rate diminishes over time until heat generation stabilizes. Most of the heat is produced in the early ages, and the chemical composition remains relatively constant from 14 to 182 days [3]. At an

✉ Yang Lu
yanglufrank@boisestate.edu

Md Asif Rahman
mdasifrahman@u.boisestate.edu

Tianjie Zhang
tjzhang@u.boisestate.edu

[1] Department of Computer Science, Boise State University, 1910 University Drive, Boise ID 83725-2060, USA

[2] Department of Civil Engineering, Boise State University, 1910 University Drive, Boise ID 83725-2060, USA

early age, heat capacity impacts heat generation, the heat of vaporization manages water phase changes, and thermal conductivity influences efficient heat transfer and hydration progress, manipulating the temperature-dependent characteristics of cement-based materials. These properties influence the degree of hydration, setting time, and strength development in concrete. Consequently, significant temperature fluctuations within the first few hours can lead to concrete domain shrinkage, reducing its strength [4]. High ambient temperatures can also accelerate evaporation and increase water demand, resulting in rapid hydration, faster setting, and reduced long-term strength [5–7]. The reduction in strength affects both concrete stiffness and fracture energy, leading to the formation of cracks [8, 9]. Therefore, it is crucial to develop tools for predicting and monitoring cement hydration kinetics to mitigate these issues. Inaccurate predictions of cement hydration temperature can lead to issues like variable strength, setting delays, cracking, and durability concerns in the construction industry. Unpredictable hydration may also result in workability challenges and temperature-related problems. Some real-world examples of such issues stemming from inaccurate cement hydration predictions include concrete cracks caused by drying shrinkage and settlement [10–16], typically initiating within 3 to 56 days after concrete placement. A comprehensive modeling framework can offer a promising avenue to gain deeper insights into the cement hydration kinetics in this regard.

Numerous researchers have employed numerical and physics-based modeling to simulate cement hydration kinetics and microstructure [17–19]. These models often rely on solving mathematical equations describing reaction and diffusion mechanisms [17–19]. Some modeling approaches incorporate physical phenomena such as diffusion, heat transfer, and water–binder ratios, solving PDEs to evaluate temperature distribution and hydration rates in cement paste [19–23]. However, constructing such predictive models involves dealing with computational challenges due to intricate mesh structures, complex mathematical derivations, and the reliance on precise phase composition and micro-scale geometry in traditional finite element solvers. Existing finite element cement hydration models exhibit limitations in accurately predicting temperature changes due to oversimplified assumptions, homogeneous material property representations, and challenges in capturing reliable hydration kinetics variability. Issues related to realistic thermal boundary conditions such as curing methods, scale dependency, and inadequate experimental validation further contribute to inaccuracies. Conversely, machine learning approaches in artificial intelligence (AI) provide an alternative perspective compared to the finite element method and have gained attention in recent decades. Leveraging a random forests (RF) model allows high-fidelity predictions of the time-dependent hydration kinetics in ordinary Portland cement (OPC)-based systems [24]. While capable of predicting without knowledge of the underlying kinetic mechanisms, it encounters difficulties in capturing intricate nonlinear relationships and interpreting results due to the black-box nature of RF. Deep learning has gained prominence for solving complex nonlinear problems using extensive data. It has been utilized to tackle temperature-related concerns since the 1990s, starting with the use of artificial neural networks to learn about the convective heat transfer coefficient [25]. Subsequently, various neural network architectures, including convolutional neural networks (CNNs), have been employed to address heat transfer challenges [26–31]. However, these models often rely on supervised learning and require large labeled datasets for effective training, creating challenges in data acquisition and limiting their practical use in scenarios where obtaining such data is difficult or costly. In addition, some unsupervised deep-learning techniques have been applied to heat transfer problems, focusing on thermal systems like heat conduction and convection [29–31]. These models, however, lack physical guidance for temperature predictions and face challenges, including the absence of labeled data, making evaluation difficult without a ground truth. The complex and abstract representations learned by these models pose interpretability issues, and selecting appropriate hyperparameters can be challenging. Overfitting, scalability issues, and sensitivity to initialization further contribute to the difficulties. Recent advancements in deep learning center on accurately estimating the remaining useful life (RUL) for engineered systems, enhancing prognostics to predict potential fatal failures due to aging or unexpected incidents [32–35]. The synergy between reinforcement learning and neural networks enhances the accuracy and adaptability of such systems [32]. High prognostic accuracy on the RUL estimation is achieved by using deep convolution neural networks [33] and hybrid deep long short-term memory networks [34]. Nevertheless, challenges such as limited labeled data, interpretability, real-time constraints, transferability concerns, and the necessity for continuous learning persist. Incorporating domain knowledge, addressing imbalanced data, and managing resource-intensive models are pivotal for effective applications in complex OPC-based system kinetics. This necessitates an essential multitask learning approach aligned with the cement hydration physics in OPC. A novel deep-learning framework, known as a physics-informed neural network, emerges as a promising solution in this regard [36]. PINN is a data-driven approach that integrates relevant physics into the learning process [36]. It solves PDEs by minimizing the residuals of these equations through a loss function, making it effective with a relatively small amount

of training data [36]. PINN has shown success in solving PDEs and has been applied to various temperature problems, including multi-physics scenarios and natural convection [37–42].

Within the above context, the research gap in cement hydration predictions stems from the intersection of traditional finite element models, machine learning, and the development of physics-informed neural networks. While finite element models lack accuracy for complex processes like cement hydration, machine learning models lack precision. As such, this work develops the PINN-CHK model, a physics-informed neural network for cement hydration kinetics that bridges the research gap by combining deep learning with physical constraints. The industry demands highly accurate and adaptable models capable of predicting cement properties under diverse conditions, making this integrated approach crucial for meeting industry needs. PINN-CHK predicts early-age adiabatic temperature rise in OPC-based cement hydration by leveraging experimental data for training [43, 44]. The adiabatic condition signifies a thermodynamic process occurring without the transfer of temperature or mass between the system and its environment. The fully connected neural network (FC-NN) is designed to capture cement hydration data and PDE-based governing equations under specified initial and boundary conditions. This achieves mesh-free simulation by embedding physical laws into the model's loss function, reducing data requirements. A feed-forward network (FNN) is trained to enable temperature prediction accommodating various initial curing temperatures. Xavier initialization and the limited-memory quasi-Newton method, L-BFGS optimizer are employed for model optimization. Applying the Xavier initialization method determines initial weights and biases, leading to improved convergence speed. The efficiency of the established model is explored by applying a hyperbolic tangent activation function Tanh. Gradients are calculated using the auto-differential technique. The model's differentiability concerning input coordinates and free parameters enables the capture of temperature evolution at various spatiotemporal scales.

The trade-off between data and physics is a pivotal consideration in the PINN-CHK model development context. This work highlights the trade-off between data-driven and physics-based approaches and emphasizes the importance of incorporating a priori knowledge to reduce data requirements. It is worth noting that the training set of the PINN-CHK model comprises only 5% of the complete dataset. This is achieved by introducing learning biases through a judicious selection of loss function, constraints, and inference algorithms that can modulate the training phase of a PINN-CHK model to explicitly favor convergence toward solutions aligned with the underlying cement hydration physics. This approach employs temperature PDEs, thermal conductivity, equivalent age, and concrete maturity equations, along with data, to train a deep neural network (DNN) representing space–time-dependent hydration temperature fields. The proposed PINN-CHK model's performance is then rigorously assessed through a comparative analysis, wherein it is juxtaposed against data-centric methods, notably a naïve DNN without any consideration of physics. A series of ablation analyses are undertaken to delve into the efficiency of PINN-CHK architectures and the influence of training data on the model's performance. The model monitors optimization complexity and visualizes weight hyperparameters, thereby emphasizing the success of using reduced training data. A robust validation against experimental data justifies the model's performance in a one-dimensional mesh-free domain. Finally, this work presents hydration temperature results under three different initial curing temperatures and subsequently defines the space–time development of concrete maturity and strength.

In summary, this work proposes the PINN-CHK model as an innovative and efficient simulation platform for understanding cement hydration kinetics and early-age temperature evolution with limited training data and without complex numerical techniques. This innovation provides a learning algorithm for concrete maturity and strength, which can be integrated into a wide range of hybrid approaches tailored to physics-informed learning systems in cement-concrete research, attaining resilient and high-fidelity predictions across diverse scientific and engineering domains.

2 Modeling and computational methods

This work develops the PINN-CHK prediction model concerning the governing equations of cement hydration kinetics. The mathematical notations used in the PINN-CHK development are summarized in Table 1.

2.1 Cement hydration kinetics

Cement hydration kinetics is a multifaceted process by which Portland cement gains its strength through chemical reactions with water. These reactions can be described by Eq. (1) [45–49], which represents the pertinent chemical transformations of the mineral constituents in Portland cement during the hydration process.

$$\begin{aligned} 2C_3S + 6H &\rightarrow C_3S_2H_3 + 3CH \\ 2C_2S + 4H &\rightarrow C_3S_2H_3 + CH \\ C_3A + CSH_2 + 10H &\rightarrow C_4ASH_{12} \\ C_4AF + 2CH + 10H &\rightarrow C_6AFH_{12} \end{aligned} \tag{1}$$

Table 1 Symbolic lexicon for PINN-CHK development

	Variables
x	Spatial coordinate
y	Spatial coordinate
t	Temporal coordinate
T	Temperature
α	Degree of hydration
$T(x, t)$	Approximate solution
$\hat{T}(x,t)$	Predicted temperature
	Parameters
ρ	Concrete density
k	Concrete thermal conductivity
c_p	Heat capacity at constant pressure
w/c	Water–binder ratio
Q	Heat of hydration or heat generation rate
E	Activation energy
R	Universal gas constant
$T(x, 0)$	Initial temperature
T_r	Reference temperature
α_u	Ultimate degree of hydration
β	Hydration shape parameter
τ	Age parameter
t_e	Equivalent age
H_u	Ultimate heat of hydration
C	Total amount of cement
t_1	Time parameter
M	Concrete maturity
S	Compressive strength
S_∞	The ultimate strength of concrete
M_0	Offset maturity
A	Regression coefficient
W	Weight matrix
b	Bias vector

where the major compounds of cement, i.e., tricalcium silicate C_3S, dicalcium silicate C_2S, tricalcium aluminate C_3A, tetracalcium aluminoferrite C_4AF, and gypsum CSH_2, go through some series of reactions to produce calcium hydroxide *CH*, ettringites, and heat release in the system. Calcium hydroxide is generated in substantial quantities during cement hydration. *CH* is water-soluble and can leach out, resulting in increased porosity, particularly in hydraulic structures. It also reacts with sulfates present in soil or water to form calcium sulfate, initiating a detrimental process known as sulfate attack. Mitigating the adverse impacts of *CH* by reducing its content in concrete and converting it into cement-based products represents a significant advancement in cement-concrete technology.

The amount of *CH* produced during the hydration of cement paste is directly proportional to the degree of cement hydration [50, 51]. By quantifying the degree of hydration using Eq. (1), it is possible to measure both the *CH* content and the associated heat production. Additionally, the maturity concept hinges on the understanding that the progress of hydration reactions is influenced by temperature. By recording temperature and time data at various locations within a concrete structure, it becomes feasible to calculate a maturity value that accounts for the cumulative temperature effect on hydration. Consequently, this work formulates a thermal equation based on the maturity equation, which incorporates the degree of cement hydration. This governing equation proves instrumental in predicting the time-dependent kinetics of cement hydration.

2.2 Governing equations

This work employs one-dimensional heat transfer principles to model the temperature rise during cement hydration. This implies that the cross-sectional area of the cement paste domain remains consistent in the direction of heat flow, and there is no heat dissipation from the sides of the simulation domain. Based on the energy conservation theory, the heat transfer equation in cement hydration can be defined by Fourier's law as follows:

$$\rho c_p \dot{T} = \nabla \cdot (k \nabla T) + Q \tag{2}$$

where ρ is the density (kg/m^3), c_p is the heat capacity (J/kg-K), T denotes temperature (K), k is the thermal conductivity (W/m–K), and Q is the heat of hydration or heat generation rate (W/m^3). Heat capacity at constant pressure is calculated from the sum of the individual components of cement paste, i.e., cement, sand, water, and chemically bound water [1, 22].

The rise in temperature during the hydration process can be represented by Eq. (3), defining the concept of equivalent age [52, 53]. With each alteration in temperature, a corresponding new equivalent age or time is determined [52].

$$\dot{t_e} = \exp\left[\frac{E}{R}\left(\frac{1}{T_r} - \frac{1}{T}\right)\right] \tag{3}$$

where t_e stands for the equivalent age at the initial curing temperature, E is the activation energy (J/mole), R is the universal gas constant (8.314 J/mole-K), and T_r is a reference temperature (K).

The maturity equation establishes a relationship between the equivalent age and the degree of hydration α [52, 54]. It is presented in Eq. (4), facilitating the monitoring of the advancement of the chemical reaction between water and cement.

$$\dot{\alpha} = \exp\left[\frac{E}{R}\left(\frac{1}{T_r} - \frac{1}{T}\right)\right]\frac{\alpha_u \beta}{t_e}\left(\frac{\tau}{t_e}\right)^{\beta}.\exp\left[-\left(\frac{\tau}{t_e}\right)^{\beta}\right] \quad (4)$$

where α_u is the ultimate degree of hydration, β denotes the hydration shape parameter, and τ is the age parameter or the hydration time (hours). From here, the heat generation rate Q can be calculated through the following relationship as in Eq. (5).

$$Q = H_u C\dot{\alpha} \quad (5)$$

where H_u is the ultimate heat of hydration (J/kg) and C is the total amount of cement (kg/m^3).

The ultimate degree of hydration α_u can be calculated based on the water–binder ratio w/c as in Eq. (6) [55].

$$\alpha_u = \frac{1.031 w/c}{0.194 + w/c} \quad (6)$$

The hydration time τ can be calculated from the equivalent age t_e, and time parameter t_1 as shown in Eq. (7) [56].

$$\tau = 1 + \frac{t_e}{t_1} \quad (7)$$

Starting here, concrete maturity serves as an indicator of the progress of curing. It reflects the interplay of concrete temperature, time, and the gain in strength. These maturity values can be determined through the application of the Nurse-Saul equation [57]:

$$M = \sum_{0}^{t} (T - T_r).\Delta t \quad (8)$$

where M represents the concrete maturity at age t (°C-hours), and Δt is the time interval (hours). The reciprocal formulation can establish the relationship between strength and maturity, as shown in Eq. (9) [58].

$$\frac{1}{S(t)} = \frac{1}{S_\infty} + \frac{1}{A}.\frac{1}{(M - M_0)} \quad (9)$$

where S is the compressive strength at time t (MPa), and S_∞ denotes the ultimate strength, i.e., compressive strength after 28 days of curing (MPa). The offset maturity M_0 implies that the strength of concrete does not begin to develop until a certain amount of maturity is reached.

2.3 Data preparation

PINN-CHK attempts to model cement hydration temperature from an initial curing temperature of 10 °C (283.15 K) and a surface temperature of 70 °C (343.15 K), learning from the experimental data [43, 44]. The data is partitioned into training and testing sets for the development of the model. Various data points, representing 1%, 5%, 10%, and 20% of the training data, are selected at different locations and times. They are randomly sampled to avoid over-representation of any specific conditions. Table 2 presents the statistical distribution of these data points to identify the significance of dataset selection and their representativeness compared to the experimental data.

Both train and test data share similar statistical characteristics with the experimental data in terms of statistical measures such as minimum, maximum, and standard deviation. This indicates that the training dataset is comprehensive and not biased, covering a wide range of conditions and temperature values relevant to experimental cement hydration. The selected train and test datasets are drawn from the same distribution as the experimental data and can be representative of diverse real-world scenarios. It is important to highlight that a model trained on a dataset that closely matches the statistical characteristics of the original data is more likely to generalize well to new, unseen data. This supports the choice of dataset selection in the PINN-CHK model development. The trained model will be validated further in later sections to justify these selections.

During network training, a total of 10,000 collocation points is utilized. Collocation points in PINN-CHK act as anchor points where the neural network learns to approximate the solution while respecting the cement hydration physics encoded in the governing equations. To facilitate the effective training of the model, the preprocessing step of this work involves min–max scaling as expressed in Eq. (10).

$$X = \frac{X - l_b}{u_b - l_b} \quad (10)$$

Table 2 Descriptive statistics of the dataset

	Variables	Min	Max	Mean	Std
	Experimental data	1.0	180.0	90.5	52.11
t(hours)	Train data	1.0	180.0	60.77	53.81
	1% train data	1.0	162.0	54.0	63.33
	5% train data	1.0	176.0	70.07	57.41
	10% train data	1.0	176.0	70.45	55.88
	20% train data	1.0	179.0	59.51	53.50
	Test data	1.0	180.0	70.5	46.55
T(°C)	Experimental data	10	70.25	59.68	17.18
	Train data	10	70.25	48.88	25.54
	1% train data	10	69.88	46.64	26.08
	5% train data	10	70.18	51.08	25.70
	10% train data	10	70.18	52.44	24.02
	20% train data	10	70.25	47.90	25.69
	Test data	10	70.25	59.68	17.18

where X represents feature values, l_b is the lower bound, and u_b is the upper bound of the feature. This operation normalizes temperature as well as spatial and temporal values to a range between 0 and 1. It is important to ensure that the bounds are appropriately chosen based on the characteristics of the original data. In this case, they are chosen based on the minimum and maximum values of the dataset. This ensures that all values are on a similar scale, addressing issues of sensitivity to feature magnitudes in the PINN-CHK network. It will help the optimization algorithm to find the minimum of the loss function more efficiently. It can lead to faster convergence during the training of PINN-CHK. The discussion on model convergence and weight distributions in each layer of the neural network, as outlined in Sect. 3, can underscore the importance of the preprocessing step in this work.

2.4 Physics-informed neural network

In this work, PINN is programmed to initiate data-driven solutions of partial differential equations. PINN-CHK is being designed to connect hydration physics to the deep neural network. In the context of PINN, a nonlinear PDE can be represented in a general form, as shown in Eq. (11).

$$T(x,t)_t + N[T(x,t)] = 0, x \in \Omega, t \in [0,T] \tag{11}$$

where $T(x, t)$ is the latent solution of the system, which is expressed as a function of space x, for some time t, within a given period $[0, T]$; x and t are the spatial and temporal coordinates, respectively; Ω and $\partial\Omega$ denote the computational domain and the boundary, respectively; $T(x, t)_t$ denotes the derivative of $T(x, t)$ concerning time t; N is called as a nonlinear differential operator. Here, x is an independent variable defined over the domain, Ω.

The data-driven solution of the above PDE can be done by defining a physics-informed neural network $f(x, t)$ as shown in Eq. (12).

$$f(x,t) = T(x,t)_t + N[T(x,t)] = 0 \tag{12}$$

In this approach, the function $T(x, t)$ is approximated using a deep neural network, denoted as $f(x, t)$, creating a PINN. Automatic differentiation is applied to compute the derivatives of the network. Subsequently, the parameters associated with both $T(x, t)$ and $f(x, t)$ are learned through the minimization of a loss function. The developed PINN-CHK takes into account various factors such as the water–binder ratio, cement paste mixing properties, chemical components of cement, and the initial curing temperature to analyze their effects on the hydration reaction.

2.4.1 PINN-CHK architecture

PINN-CHK attempts to capture the early-age temperature evolution during cement hydration, in a deep-learning framework. The successful PINN architecture requires achieving a perfect structure of the deep neural network, including the number of layers, the number of neurons in each layer, etc. The construction utilizes neural networks to incorporate cement hydration knowledge, experimental data, and physical constraints from a system of ordinary and partial differential equations. The FC-NN fosters interconnections between neurons in different layers while training the network for predicting cement hydration temperatures. In essence, the PINN-CHK architecture comprises two core components: a deep neural network and a physics-informed neural network. A schematic diagram of the developed PINN-CHK for solving the cement hydration temperature is presented in Fig. 1. A one-dimensional cement paste domain representing one arm (100 μm) of the domain cross-Sect. (100×100 μm^2) is considered, to model the cement hydration temperature.

PINN-CHK employs a 3-layer neural network with 24 neurons in each layer for supervised learning using experimental cement hydration data, adopting an FNN based on the PINN framework [36]. Here, FC-NN is used for solving cement hydration temperature by building up inputs (x) and output (y) relations. The neural network can be composed of multiple hidden layers, where the inputs ($X = [x_1, x_2, \ldots, x_i]$) in each hidden layer produce some outputs ($Y = [y_1, y_2, \ldots, y_j]$), through the FC-NN network. The process can be demonstrated as follows:

$$y_j = \sigma\left(w_{i,j}x_i + b_j\right) \tag{13}$$

where $w_{i,j,}$ and b_j are the trainable weight matrix and bias vector, respectively; $\sigma(.)$ is the activation function which enables the nonlinear transformation of information through the neurons in each hidden layer. This work adopts a hyperbolic activation function, as illustrated in Eq. (14).

$$\mathrm{Tanh}(x) = \frac{e^x - e^{-x}}{e^x + e^{-x}} \tag{14}$$

Here, the hyperbolic tangent Tanh is a nonlinear activation function, which is taken to prevent linearity [59]. This enables nonlinear temperature data to pass through the nodes and layers of the network. It is needed to initialize the model parameters at first, for this four-layer network. The Xavier initialization method is applied to decide the initial weights and biases in the network [60]. This method helps to set the output variance of each layer close enough, which will enhance the convergence process and better information flow through the network. Thus, a network with L layers has to process the Linear to Tanh forward function L-1 time for the layers 1 through L-1. The identity

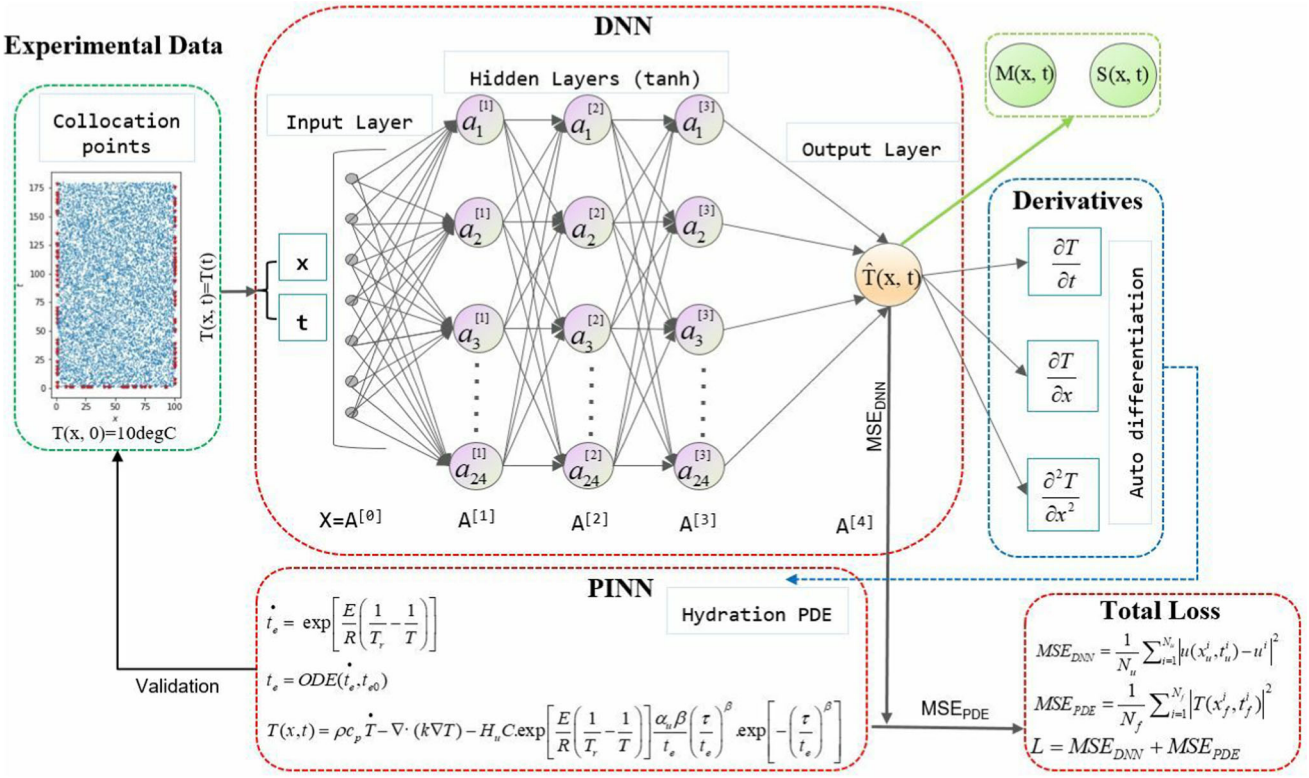

Fig. 1 Schematic of the PINN-CHK architecture developed for the cement hydration kinetics prediction

function, a linear activation function is added at the end for the output layer L. The identity function helps to predict temperature as a continuous variable. Thus, it enables an L-model forward function. The following equation set describes the design of the forward propagation module in PINN-CHK.

$$\begin{aligned} z^{[1](i)} &= W^{[1]}x^{(i)} + b^{[1]} \\ a^{[1](i)} &= \tanh\left(z^{[1](i)}\right) \\ z^{[2](i)} &= W^{[2]}a^{[1](i)} + b^{[2]} \\ a^{[2](i)} &= \tanh\left(z^{[2](i)}\right) \\ &\cdots\cdots\cdots\cdots \\ z^{[5](i)} &= W^{[5]}a^{[4](i)} + b^{[5]} \\ a^{[5](i)} &= I\left(z^{[5](i)}\right) \\ T^{(i)}_{\text{prediction}} &= a^{[5](i)} \end{aligned} \tag{15}$$

where the superscript [L] denotes a quantity associated with the L$^{\text{th}}$ layer, superscript (i) denotes a quantity associated with the i^{th} example. $a^{[L]}$ is the L$^{\text{th}}$ layer activation, and $W^{[L]}$ and $b^{[L]}$ are the L$^{\text{th}}$ layer parameters. Here, example $x^{(i)}$ represents the training set at the input layer. In Fig. 1, the FC-NN is used to approximate the solution of $T(x, t)$, where fully connected layers take the coordinates (x, t) as inputs, and then produce outputs $\hat{T}(x,t)$ through the neural network. Here, the information corresponding to the cement hydration temperature has been passed through this neural network. The hydration temperature experimental data is fed into the network as the initial and boundary conditions. These initial and boundary temperature values are applied to the network at different space x and time t, which are the input vectors at the input layer of the network. The corresponding vector is then multiplied by the weight matrix $W^{[L]}$ and added to the intercept $b^{[L]}$. The result is called the linear unit which carries some information from the input. Next, Tanh activation of the linear unit enables the hidden layers, to have the nonlinear transfer of the hydration temperature information from one layer to the next. The process is repeated several times for each $W^{[L]}$ and $b^{[L]}$ until it reaches the [L-1] layer. Finally, the identity function of the final linear unit is taken at the L$^{\text{th}}$ layer. Hydration temperature is a continuous variable, and thus, the output layer predicts the temperature values $\hat{T}(x,t)$ through this regression network.

The second part of PINN-CHK architecture is to initiate a solution to the hydration physics. In this part, the model attempts to estimate the temperature–time effects in cement hydration kinetics. The hydration temperature shown in Eq. (2) can be rearranged and expressed in terms of initial and boundary conditions, in this regard:

$$\begin{aligned} \rho c_p \dot{T} - \nabla \cdot (k \nabla T) - Q &= 0 \\ T(x,0) &= 10 \\ T(0,t) = T(-1,t) &= T(t) \end{aligned} \tag{16}$$

where the approximate solution $T(x, t)$ has its derivative as $T(x, t)_t = \dot{T} = \frac{\partial T}{\partial t}$. $T(x, 0)$ denotes the initial curing temperature of 10 °C at time $t = 0$, at all locations x. The temperature increases gradually with the progression of time t within a period [0, T].

Thus, the physics-informed neural network $f(x, t)$ is defined by hydration temperature as in Eq. (17), which can further be expressed as Eq. (18) by coupling Eq. (3) and Eq. (4).

$$f(x,t) = \rho c_p \dot{T} - \nabla \cdot (k \nabla T) - Q \tag{17}$$

$$f(x,t) = \rho c_p \dot{T} - \nabla \cdot (k \nabla T) - H_u C \cdot \exp\left[\frac{E}{R}\left(\frac{1}{T_r} - \frac{1}{T}\right)\right] \frac{\alpha_u \beta}{t_e} \left(\frac{\tau}{t_e}\right)^{\beta} \cdot \exp\left[-\left(\frac{\tau}{t_e}\right)^{\beta}\right] \tag{18}$$

$$t_e = \mathrm{ODE}(\dot{t_e}, t_{e0}) \tag{19}$$

where t_{e0} is the equivalent age at time 0 and t_e is the equivalent age at time t.

To solve the hydration PDEs, it is necessary to calculate the network output derivatives concerning the network input. Here, the differential operators involved in the hydration PDEs are evaluated by leveraging the automatic differentiation method [61]. Automatic differentiation applies the chain rule to compute the derivatives of the DNN output. This will help to compute the physics-based loss function without any discretization errors while training the network. Thus, the derivatives of hydration temperature $\hat{T}(x, t)$ are calculated concerning space x and time t. The temperature derivatives are then used to solve the hydration PDEs. The equivalent age is quantified through a function that solves the ordinary differential equation. Thus, PINN-CHK approximates the hydration temperature $T(x, t)$ by the hydration PDEs, at different space x and time t coordinates.

In the model development, the initial curing temperature is kept equal to the reference temperature, to confirm that no temperature gradient exists at the beginning. In this work, it is believed that the degree of hydration can vary between 0 and 1 depending on the progress of the hydration. This will identify the beginning of the hydration process and its journey until it can achieve the ultimate degree of hydration. Thus, the values of the equivalent age and the degree of hydration are considered zero initially.

The PINN-CHK is trained based on the mean-squared error (MSE) loss. The MSE loss function creates a criterion that measures the mean-squared error between each element available in the input (x, t) and target (y). The prediction is done with training data points N_u and collocation points N_f, chosen randomly at the boundary and within the one-dimensional enclosure, respectively. Here, collocation points are several points in the cement paste domain, where predicted temperature which satisfies the relevant hydration physics at those points is justified as accurate.

The model utilizes L-BFGS Optimizer to minimize the MSE loss function [62]. PINN-CHK is integrated into Python utilizing a popular machine learning package PyTorch [59]. It initializes the neural network, i.e. the layers, as a list using a container, ModuleList [59].

MSE loss is considered as a combination of the loss from the DNN and loss from the hydration PDEs. Loss from the deep neural includes the losses from both initial and boundary conditions. Thus, total loss L can be shown as in Eq. (20).

$$L = \mathrm{MSE}_{\mathrm{DNN}} + \mathrm{MSE}_{\mathrm{PDE}} \tag{20}$$

The neural network is trained by the given set of initial and boundary conditions, which contribute to the loss function through Eq. (21). This accounts for the losses generated from the DNN.

$$\mathrm{MSE}_{\mathrm{DNN}} = \frac{1}{N_u} \sum_{i=1}^{N_u} \left| u\left(x_u^i, t_u^i\right) - u^i \right|^2 \tag{21}$$

where $x_u{}^i$, $t_u{}^i$, u^i represent the training data from initial and boundary conditions.

On the other hand, the physics-informed neural network $f(x, t)$ contributes to the loss function through Eqs. (22–23). This accounts for the losses generated from the hydration PDEs.

$$\mathrm{MSE}_{\mathrm{PDE}} = \frac{1}{N_f} \sum_{i=1}^{N_f} \left| f\left(x_f^i, t_f^i\right) \right|^2 \tag{22}$$

$$\mathrm{MSE}_{\mathrm{PDE}} = \frac{1}{N_f} \sum_{i=1}^{N_f} \left| \rho c_p \dot{T} - \nabla \cdot (k \nabla T) - H_u C . \exp\left[\frac{E}{R}\left(\frac{1}{T_r} - \frac{1}{T}\right)\right] \frac{\alpha_u \beta}{t_e} \left(\frac{\tau}{t_e}\right)^{\beta} . \exp\left[-\left(\frac{\tau}{t_e}\right)^{\beta}\right] \right|^2 \tag{23}$$

where x_f^i, t_f^i represent the collocation points within the simulated domain.

It is noteworthy that MSE loss shares the same parameters between both DNN and PDE losses, which allows the neural network to learn by minimizing both losses in parallel. Thus, the structure imposed by the cement hydration equation enables physical interpretability within the deep-learning framework.

PINN-CHK is trained to fit the nonlinear cement hydration data. As such, the model is trained to find the best hyperparameters. A reasonable choice of learning rate

is the crucial hyperparameter of neural networks [63]. The model has been meticulously fine-tuned for a learning rate of 1×10^{-3} throughout 10,000 training steps.

The parameters of the fully connected network are trained using gradient descent and back-propagation of the loss function. The model updates these parameters based on the gradients derived from the back-propagation process. The trained parameters are then used to make predictions. This iterative process continues until the losses reach a minimum, and the model's predictions align with the experimental data. Consequently, once trained, PINN-CHK can effectively generate physically informed forecasts of cement hydration temperature at the output layer. The anticipated temperature can also be leveraged to determine the progression of concrete maturity and strength.

2.4.2 PINN-CHK model validation

PINN-CHK is designed to validate against the experimental data of early-age temperature rise [43, 44]. The mixing properties of cement paste must be aligned with the experimental setup. To do so, an OPC400 specimen containing 400 kg/m^3 of cement content and a water–binder ratio of 0.392 are taken into consideration [1]. The model learns from an initial curing temperature of 10 °C and then extrapolates the predicted hydration temperature for other initial curing temperatures in the input. The details of the model parameters and the relevant material properties are presented in Table 3. The model prediction continues over 180 h to evaluate the early-age temperature rise in cement paste.

To evaluate the performance of the developed PINN-CHK in inferring the hydration temperature, the results from PINN-CHK are compared to the experimental results. The spatial assessment relied on performance metrics including root mean square error (RMSE) as follows:

Table 3 Material properties and the model parameters

	Values	Source
Concrete density, ρ	2349 [kg/m^3]	Calibrated
Concrete thermal conductivity, k	2.6 [W/m–K]	Calibrated
Heat capacity at constant pressure, c_p	9020[J/Kg-K]	[1]
Activation energy, E/R	5000[K]	[1]
Hydration shape parameter, β	1.52	[56]
Total heat of hydration, H_u	385,000 [J/Kg]	[56]
Time parameter, t_1	13	[56]
The ultimate strength of concrete, S_∞	27.4 [MPa]	Calibrated

$$\mathrm{RMSE} = \sqrt{\frac{1}{N}\sum_{i=1}^{N}(y^i - p^i)^2} \tag{24}$$

where, N is the number of data, and y^i and p^i represent the observed and predicted values, respectively. RMSE is a statistical measure that quantifies the average magnitude of the errors. Typically, lower RMSE values correspond to reduced discrepancies between the experimental and predicted values, signifying the accuracy of the models.

The average of the space–time prediction of temperature $\hat{T}(x,t)$ from the trained PINN-CHK is plotted against the experimental data. This work uses absolute errors in many cases to highlight the model performance:

$$\varepsilon_T = \left|T - T_{\exp}\right| \tag{25}$$

where ε_T is the absolute error between the predicted temperature T and experimental temperature T_{exp}. Incorporating experimental data into the network enables a supervised learning task. Calculated as the absolute difference between predicted and experimental values, absolute errors provide insights into how well the model adheres to physics-driven constraints. Their interpretability, robustness against outliers, and scale independence make them suitable for communicating performance to stakeholders.

Moreover, this work uses relative L2 error as the metric in model validation:

$$\varepsilon_T = \frac{\left\|T - T_{\exp}\right\|_2}{\left\|T_{\exp}\right\|_2} \tag{26}$$

where ε_T is the relative L2 norm of the error, $\left\|T - T_{\exp}\right\|_2$ is the L2 norm of the prediction deviation of temperature at a certain time, and $\left\|T_{\exp}\right\|_2$ denotes the L2 norm of the experimental data at that time. This metric will provide a good quantification of the prediction accuracy at any certain time.

3 Results and discussion

This work delves into the temporal changes in temperature during the early ages of cement paste hydration. This is to reconstruct the cement hydration temperature from the experimental data, for an initial curing temperature of 10 °C. Obtaining data at fixed locations makes it relatively straightforward to measure physical parameters. As such, continuous time data at fixed spatial points are fed into the developed PINN-CHK network. Figure 2 illustrates these points for 1%, 5%, 10%, and 20% training data at different spaces and times. The selection of these training sets is based on the calibration in training the network. Here,

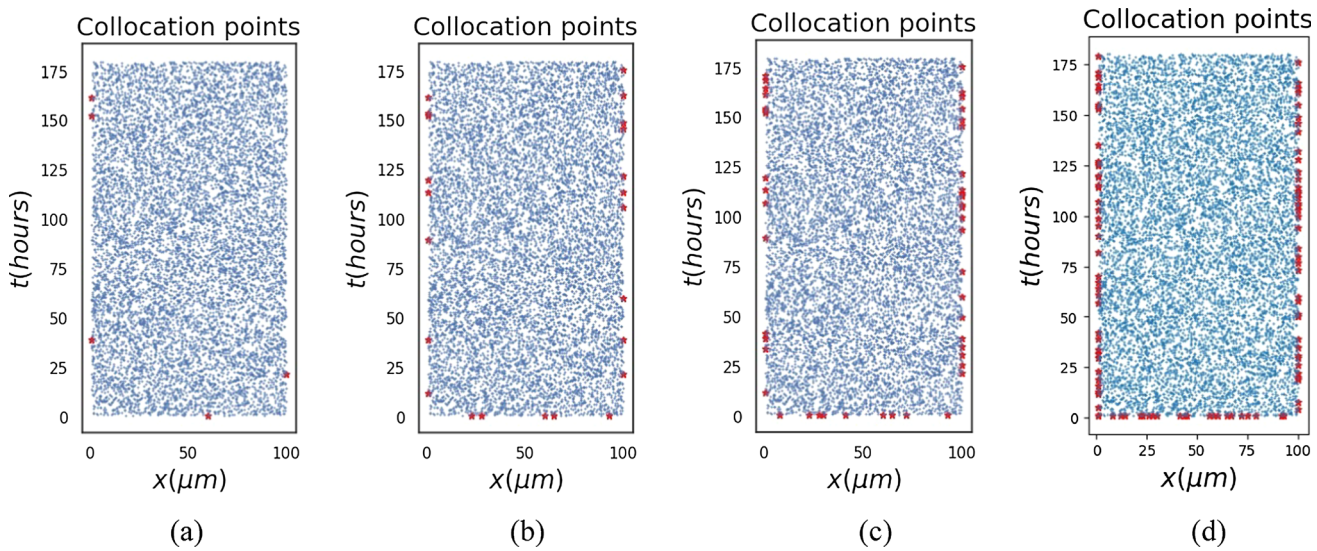

Fig. 2 Training points: **a** 1% train data, **b** 5% train data, **c** 10% train data, and **d** 20% train data

x denotes the space where the location ranges from 0 to the domain size of 100 μm, and t is the time in hours which ranges from 0 to the model prediction period of 180 h. Red colored dots denote the training temperature data chosen randomly at the boundary. Blue colored dots are the collocation points chosen randomly inside the domain.

It is required to train the network effectively to make reasonable predictions from the developed PINN-CHK. As such, the tuned model has been employed to generate temperature predictions across various locations corresponding to different training data points within the cement paste domain. Figure 3 assesses PINN-CHK's performance in solving cement hydration temperature by displaying the spatial distribution for the aforementioned collocation points. It is being compared to the naïve DNN model with an identical neural network architecture as PINN-CHK. Ground truth is defined as the experimental findings, which are used to guide the training process in the PINN-CHK through a suitable set of initial and boundary conditions. The ground-truth temperature values collected from the one-dimensional heat transfer experiment data are uniform across all positions for any specific time [43, 44]. Here, cement hydration starts with an initial curing temperature of 10 °C, which should reach to a maximum temperature of $\sim$ 70 °C at the end of 180 h, based on the experimental data. The difference between the ground truth and the model prediction is quantified by the absolute error (|ground truth-prediction|), which evaluates the model performance.

The two-dimensional visualization plot as shown in Fig. 3 compares the performance of PINN-CHK and naïve DNN models in predicting cement hydration temperature across varying training data percentages, ranging from 1 to 20%. This analysis unveils several crucial insights into model performance across various spatial and temporal locations. As the training dataset expands, the naïve DNN model gradually catches up with an RMSE of 5.33 for 20% train data, reflecting its data-driven strength. With decreasing RMSE values, the naïve DNN model significantly narrows the performance gap beyond a certain point (5% training data). These insights highlight the interplay between model architecture, data availability, and predictive capabilities. However, the naïve DNN model lacks precision in predicting cement hydration kinetics and physical patterns, exhibiting absolute errors as high as 40–50 °C. Conversely, the PINN-CHK model displays remarkable robustness when the training dataset is limited, offering more reliable predictions with scarce data. Looking at the RMSE values, this work identifies the existence of a 'threshold effect' in terms of training data, where beyond a certain percentage, further data acquisition yields no improvements in PINN-CHK model performance. In this scenario, PINN-CHK demonstrates optimal behavior with just 5% of training data having an RMSE as low as 0.88. Hence, on average, PINN-CHK predictions deviate by approximately 0.88 °C from the experimental data, which is very low compared to the mean temperature of 59.68 °C as described in Sect. 2.3. This leads to a negligible absolute error (|ground truth—prediction| $\sim$ 0), indicating enhanced accuracy for the model trained with 5% of the data. The outcomes reveal a gradual decrease in the adiabatic temperature rise as the hydration process progresses over time. Nevertheless, once this threshold effect is surpassed, PINN-CHK fails to enhance its performance with additional training data. The RMSE values have increased to 18.79 and 20.92 for 10% and 20% of the training data, showing absolute error as high as 35–40 °C. This implies that there exists a trade-off between the

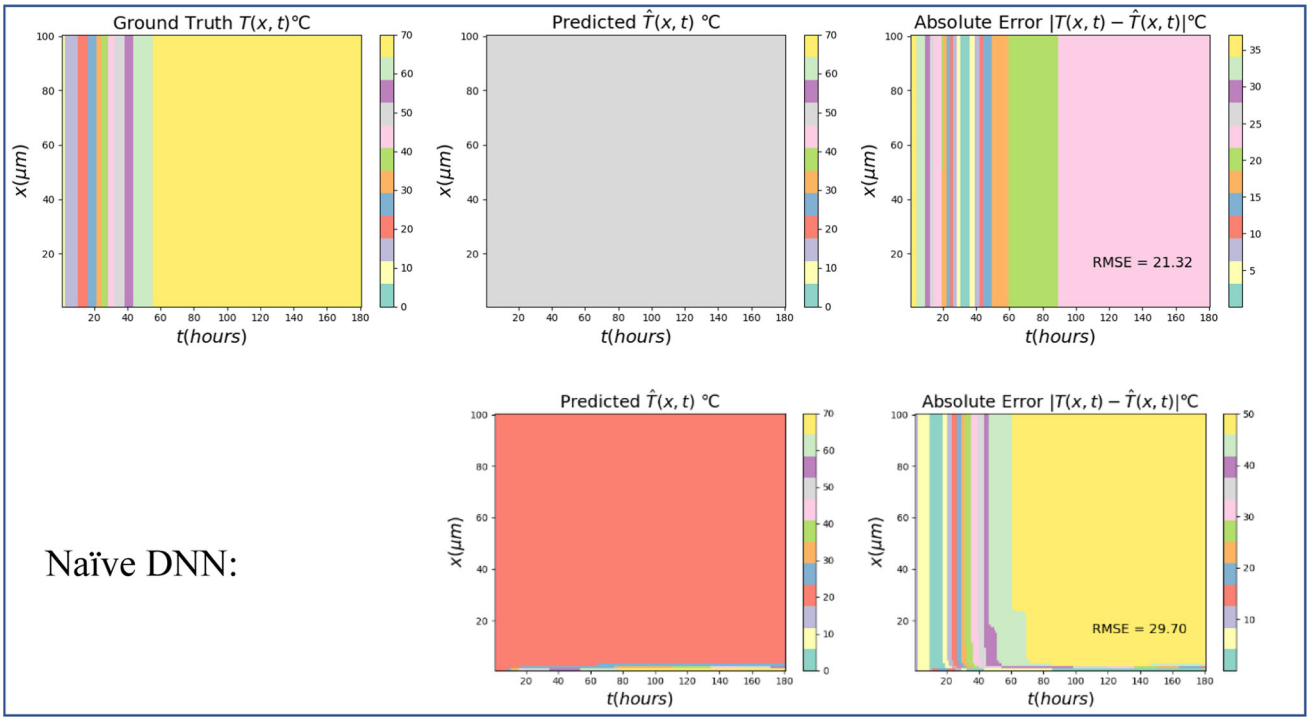

(a)

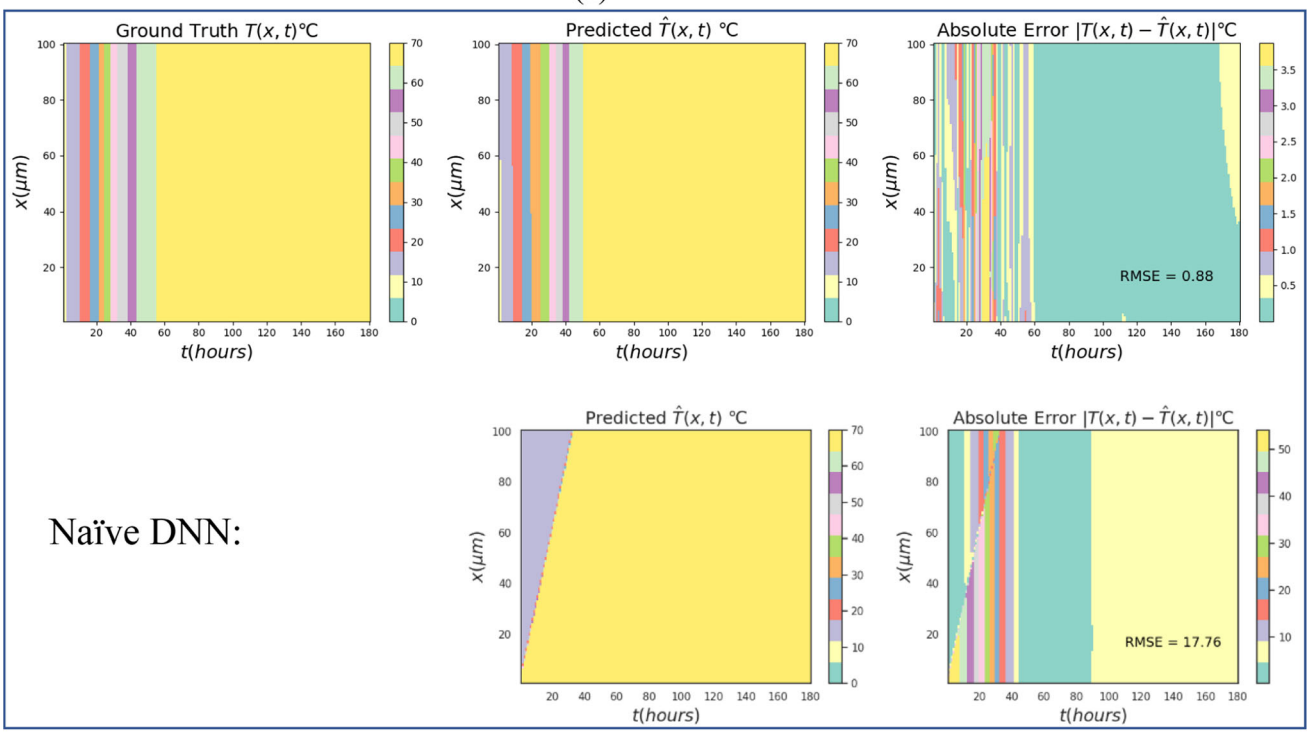

(b)

Fig. 3 Visualization of the PINN-CHK prediction for different training points: **a** 1% train data, **b** 5% train data, **c** 10% train data, and **d** 20% train data

volume of data and the comprehension of the underlying physics. The trade-off underscores the importance of balancing data efficiency and model complexity in the context of physics-informed modeling, suggesting that

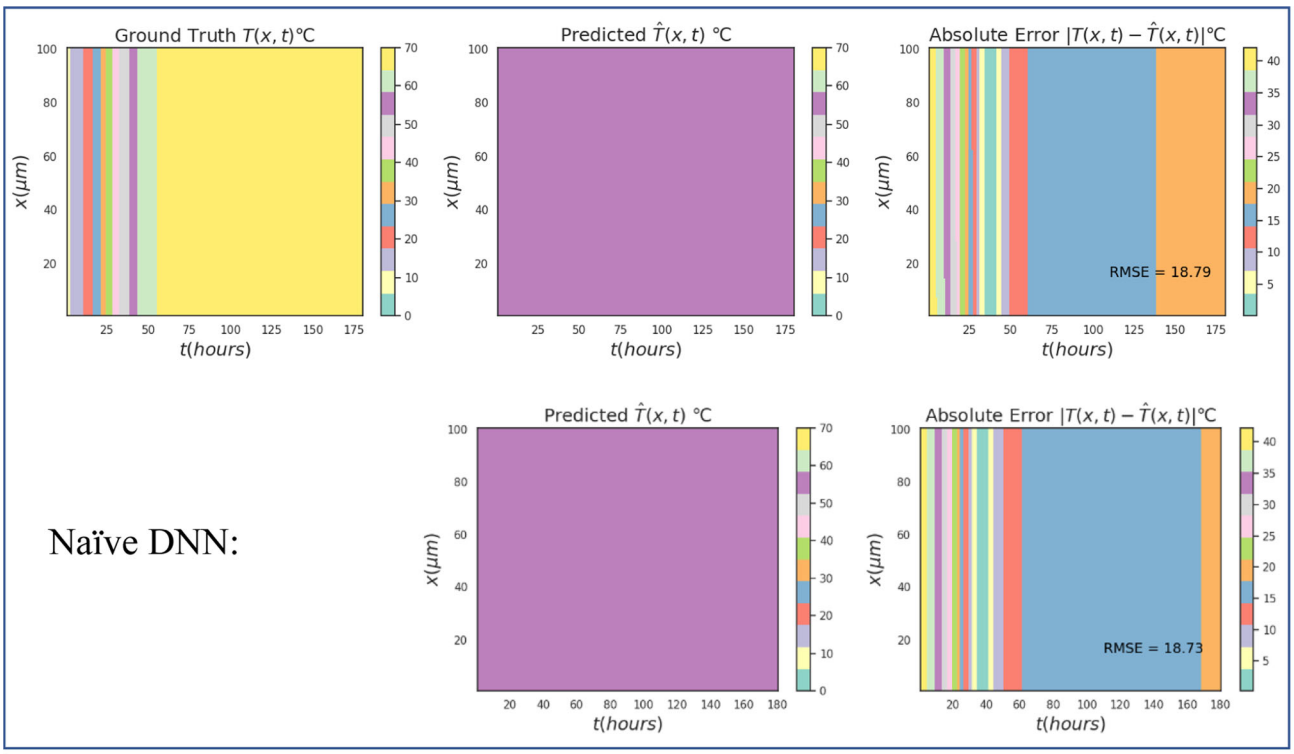

(c)

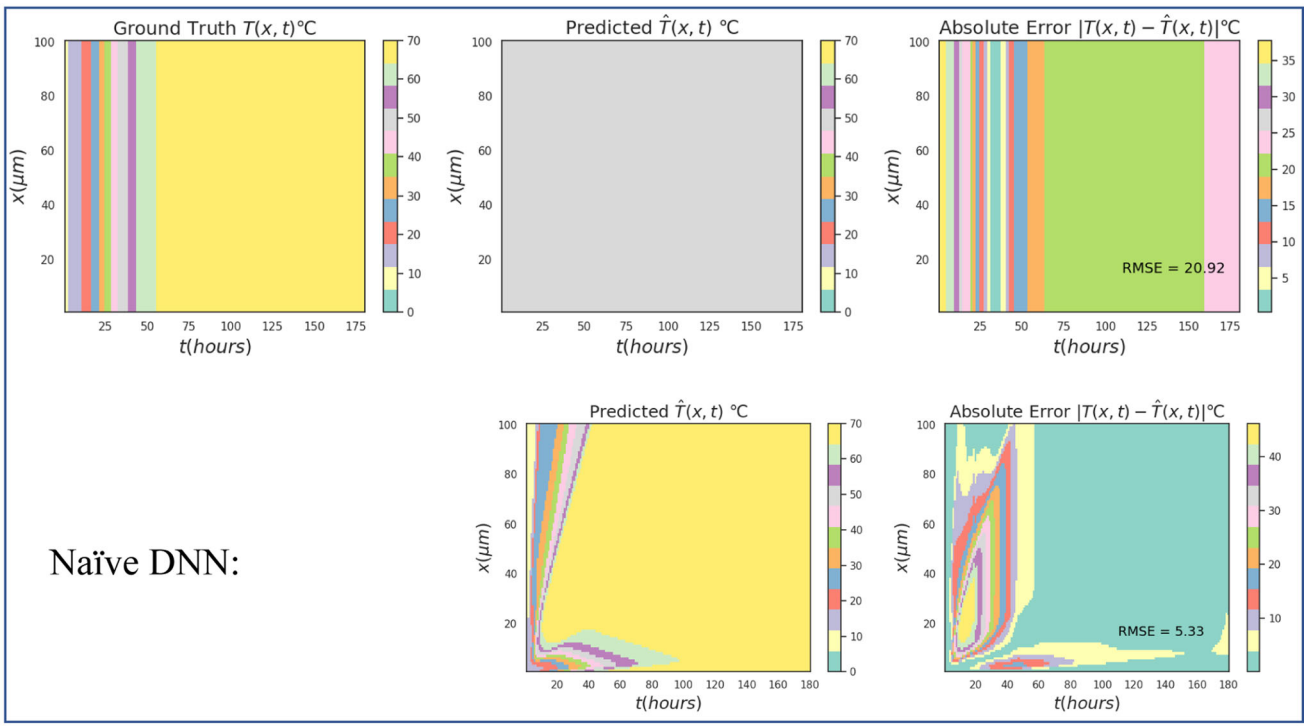

(d)

Fig. 3 continued

PINN-CHK may reach a saturation point in performance with additional data beyond that threshold, while naive DNN continues to leverage more data for improved generalization.

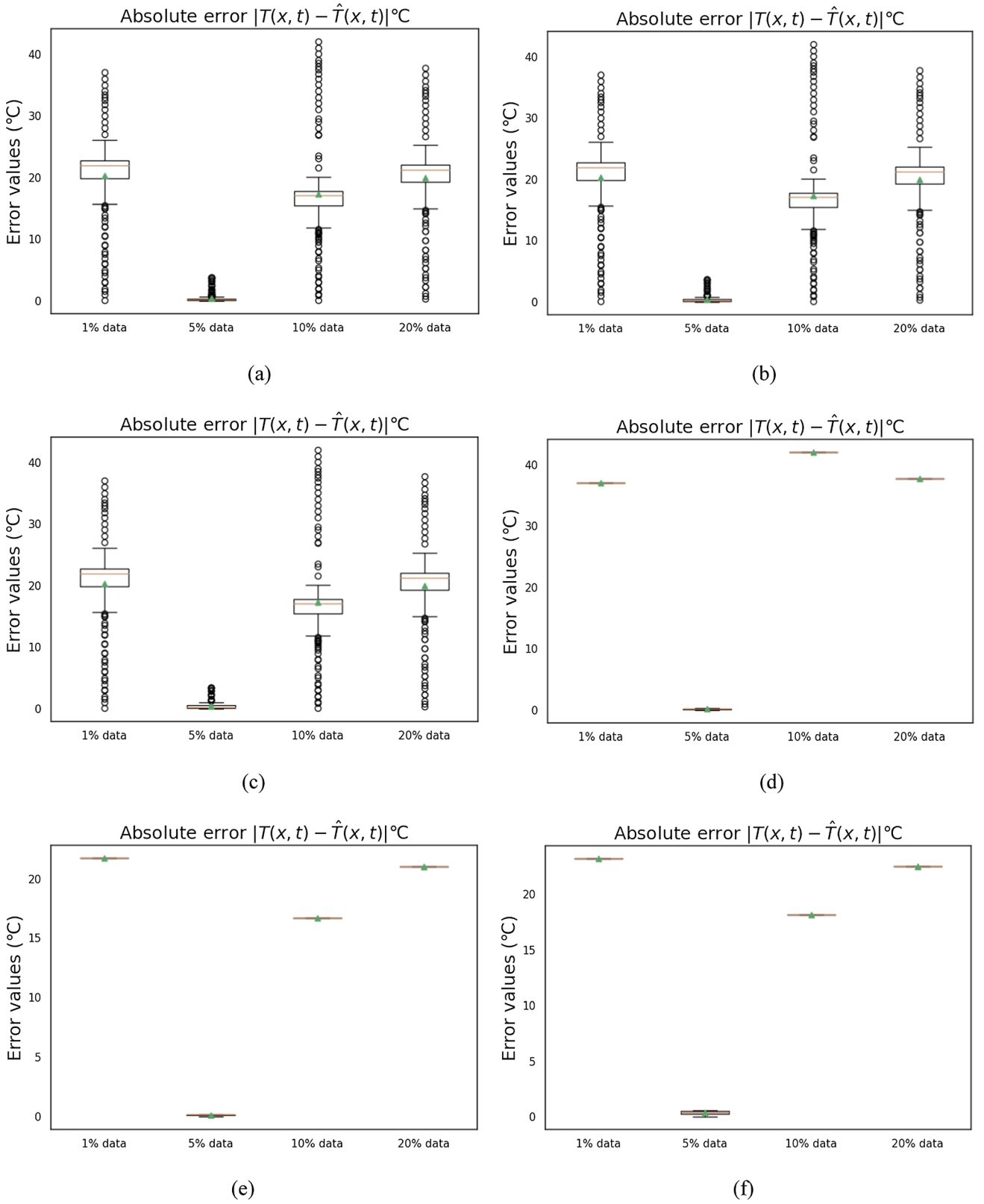

Fig. 4 Absolute errors in PINN-CHK prediction: **a** at space $x = 0$ μm, **b** at space $x = 50$ μm, **c** at space $x = 100$ μm, **d** at time $t = 0$ h, **e** at time $t = 90$ h, and **f** at time $t = 180$ h

Additional examination of the absolute errors is depicted in Fig. 4, with box plots providing a statistical representation of prediction errors in various spatial slices (x) and time instances (t).

The statistical distribution of absolute errors is visually represented through box plots as shown in Fig. 4. In these plots, the bottom of the box represents the 25th percentile, and the top of the box corresponds to the 75th percentile of the absolute error values. In this case, the median, or second quartile, is denoted by a line inside the box, while the mean value is indicated by a green triangle within the plots. Accurate predictions with minimal errors are primarily achieved with only 5% of the training data. When considering spatial slices at $x = 0$ µm, 50 µm, and 100 µm, both the mean and median closely align for predictions generated with 5% and 10% of the training data. In the case of 5% training data, a few outliers are observed, whereas 10% training data show more outliers. However, the model trained with 1% and 20% of the data exhibits numerous outliers that deviate significantly from the mean and median. On the other hand, when examining temporal slices at $t = 0$ h, 90 h, and 180 h, the mean and median values of absolute errors intersect for all predictions, whether using 1%, 5%, 10%, or 20% of the training data. However, predictions with 1%, 10%, and 20% training data exhibit larger absolute error values, while predictions generated with 5% training data display a more stable distribution of absolute errors, with values approaching zero. This suggests that predictions with 1%, 10%, and 20% training data do not align well with experimental findings and exhibit substantial variance over time. The average temperature prediction across the entire domain, as depicted in Fig. 5a, clearly demonstrates this stark contrast in performance. For an initial curing temperature of 10 °C, predictions with 1%, 10%, and 20% of the training data perform poorly, except for the 5% dataset. In contrast, predictions derived from the 5% training data exhibit strong consistency with the experimental data, as illustrated in Fig. 5b.

Figure 6 provides a more detailed representation of the comparison between PINN-CHK predictions and experimental data. This comparison specifically pertains to an initial curing temperature of 10 °C and employs a training dataset that comprises only 5% of the available data. It focuses on the adiabatic temperature test conducted on OPC400 concrete. As time progresses, the hydration temperature experiences a consistent increase, with the rate of temperature rise gradually stabilizing after 60 h. This stabilization is primarily attributed to the depletion of the chemical species involved in the hydration reaction process. In Fig. 6a, the error bars visually represent the variability in temperature data, conveying the level of uncertainty or error in the measurements. Notably, the predicted temperature values closely match the experimental data within a 5% variance, with the most significant disparities occurring during the time interval between 25 and 35 h. This time range corresponds to a critical phase of rapid cement hydration, characterized by complex physical processes. The scarcity of experimental data during this initial age makes accurate predictions challenging. However, the prediction accuracy gets significantly better beyond this critical range, with absolute error values approaching zero with the progression of time, as demonstrated in Fig. 6b.

Therefore, PINN-CHK can achieve accurate predictions with a minimal dataset, requiring as little as 5% of the

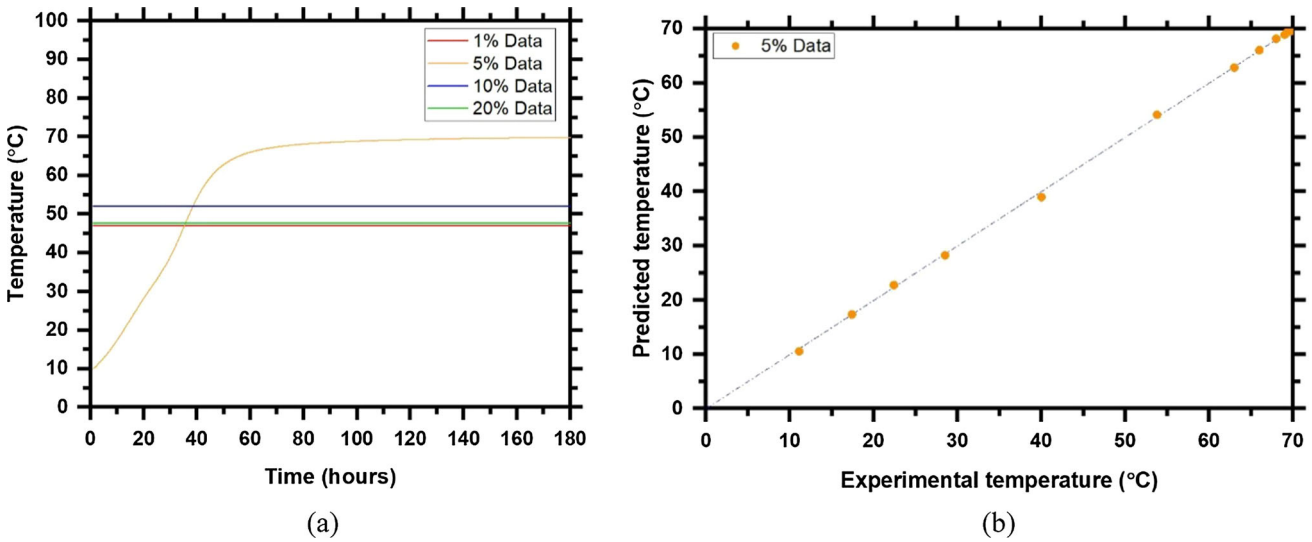

Fig. 5 PINN-CHK prediction comparison: **a** prediction results for different training sets, and **b** a comprehensive comparison with the experimental data

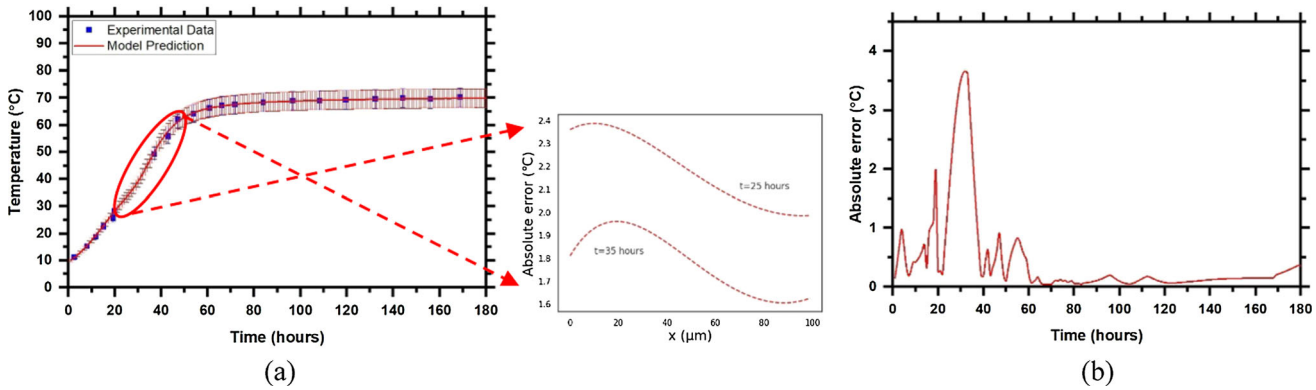

Fig. 6 PINN-CHK validation for OPC400 concrete: **a** comparison between the predicted and experimental data, and **b** absolute error

training data. It is possible to consider the weight distributions of this trained network to provide valuable insights into how neural networks are learning and processing information for cement hydration temperature prediction. Figure 7 describes the weight distribution and heat map of the trained network. A neural network with three hidden layers has four sets of weight distributions when plotting histograms of weight values. The weights are connecting one layer of neurons to the next layer. Figure 7a shows the weight distributions for each connection between layers in the neural network. This allows us to analyze how information flows and is processed through the network during training, providing insights into the network's behavior and learning process. The sparse distributions in the weights of the first layer might suggest that the neurons in the first hidden layer are not all equally active for every input feature. Some neurons may be selectively responding to specific input features or patterns. This can be a desirable characteristic because it indicates that the network is learning to extract relevant features from the input data. Sparse activations can also reduce the risk of overfitting, as the network is not over-relying on every feature. Normal distributions in the weights of the intermediate layers (2nd and 3rd) indicate that neurons in these layers are interacting with a balanced mix of inputs from the previous layer. This can be a positive sign, as it suggests that the network is maintaining a balanced flow of information through these layers. The normal distribution shape often implies that weights are symmetrically distributed around zero, which can lead to stable learning. Sparse distributions in the weights of the final layer (4th layer) suggest that not all neurons in the output layer are equally involved in generating predictions. Some output neurons may be more specialized in capturing specific patterns or features in the data. Similar to the first layer, this can be a desirable characteristic as it indicates that the network is not wasting capacity on irrelevant output neurons. However, the symmetric distributions indicate that the network is learning balanced representations.

The observed weight distributions in each layer of the neural network can be interpreted with a heat map as shown in Fig. 7b. Sparse distributions in the first and last layers suggest that the network is focusing on relevant features and patterns of the cement hydration kinetics for the input and output data, respectively. Normal distributions in intermediate layers indicate balanced information processing. Moreover, weight values are consistently bounded within reasonable ranges. These attributes are in harmony with PINN-CHK's gradual learning of the cement hydration kinetics process, as demonstrated in the validation plot presented in Fig. 6. The preprocessing step in this model development helps to achieve such improved stability while training. Understanding the contribution of each layer's weights in influencing the model's predictions not only enhances transparency but also provides a comprehensive view of how the model processes information at different levels, reinforcing the claim that the PINN-CHK model is unbiased and its decisions are based on a clear and interpretable rationale. This can be indicative of a well-trained network and good convergence toward the solution. Hence, the architecture of PINN-CHK has been designed with 3 hidden layers, each containing 24 neurons. The well-optimized PINN-CHK design, operating at a learning rate of 1×10^{-3} and trained with just 5% of the data, exhibits a minimal reliance on the data quantity.

Table 4 outlines computation times for parameter variations on the test data. Experiments on an NVIDIA RTX Laptop GPU show minimal time for temperature prediction aligned with trained model parameters. Deviations increase computation time, indicating a correlation between model parameters and speed. More training data proportionally impacts processing time. This indicates a potential correlation between the size of the training dataset and the computational demands of the physics-informed network PINN-CHK. The computation time of PINN-CHK is also

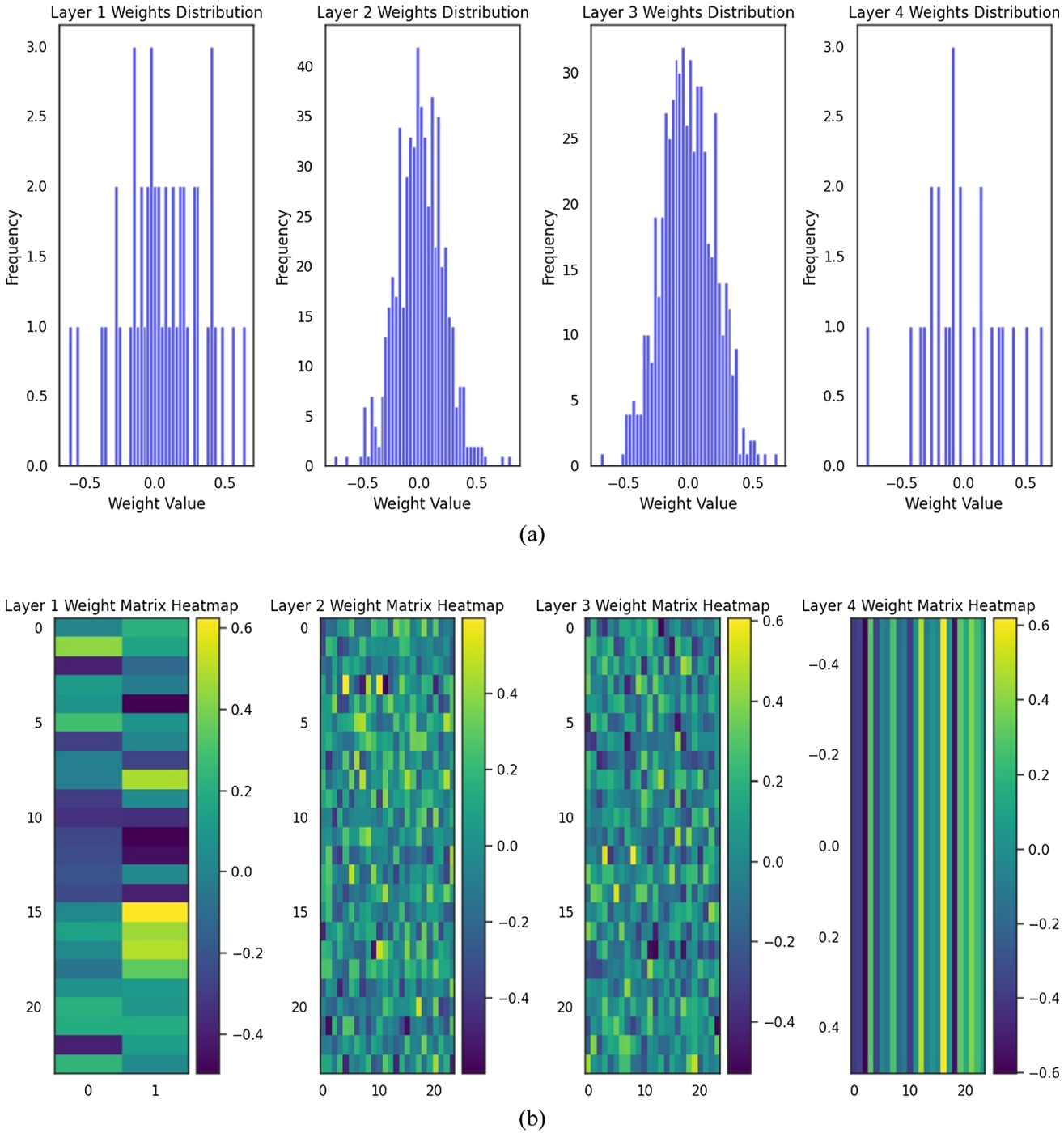

Fig. 7 Weight distributions of PINN-CHK neural network: **a** histograms and **b** heat maps

compared with a naïve DNN. PINN-CHK surpasses the naïve DNN in computation time, highlighting the efficiency gains from integrating physics-informed constraints. Performing sensitivity analyses on the parameters concerning computation time reveals the model's performance across diverse design environments, providing insights into its transferability and indicating a non-biased model. Thus, the developed PINN-CHK model with 5% train data is computationally efficient and can predict accurately without compromising the speed. Consequently, the developed PINN-CHK utilizes a 5% training dataset for subsequent analysis, predictions, and extrapolations, encompassing various initial conditions and boundary conditions.

The convergence of the PINN-CHK architecture during the prediction of cement hydration temperature is illustrated in Fig. 8 for initial curing temperatures of 10 °C,

Table 4 Computational cost and running time analysis for PINN-CHK model

Parameters	Values	Time (s)					
		PINN-CHK			Naïve DNN		
		5% data	10% data	20% data	5% data	10% data	20% data
ρ	2349 [kg/m^3]	0.031	0.048	0.085	0.068	0.093	0.105
	3000 [kg/m^3]	0.039					
	3200 [kg/m^3]	0.04					
C	300 [kg/m^3]	0.031					
	400 [kg/m^3]	0.031	0.048	0.085	0.068	0.093	0.105
	450 [kg/m^3]	0.043					
w/b	0.3	0.033					
	0.392	0.031	0.048	0.085	0.068	0.093	0.105
	0.4	0.034					
$T(x, 0)$	10 °C	0.031	0.048	0.085	0.068	0.093	0.105
	20 °C	0.034					
	30 °C	0.036					
H_u	350,000 [J/Kg]	0.054					
	385,000 [J/Kg]	0.031	0.048	0.085	0.068	0.093	0.105
	400,000 [J/Kg]	0.037					
α_u	0.626	0.033					
	0.689	0.031	0.048	0.085	0.068	0.093	0.105
	0.694	0.034					

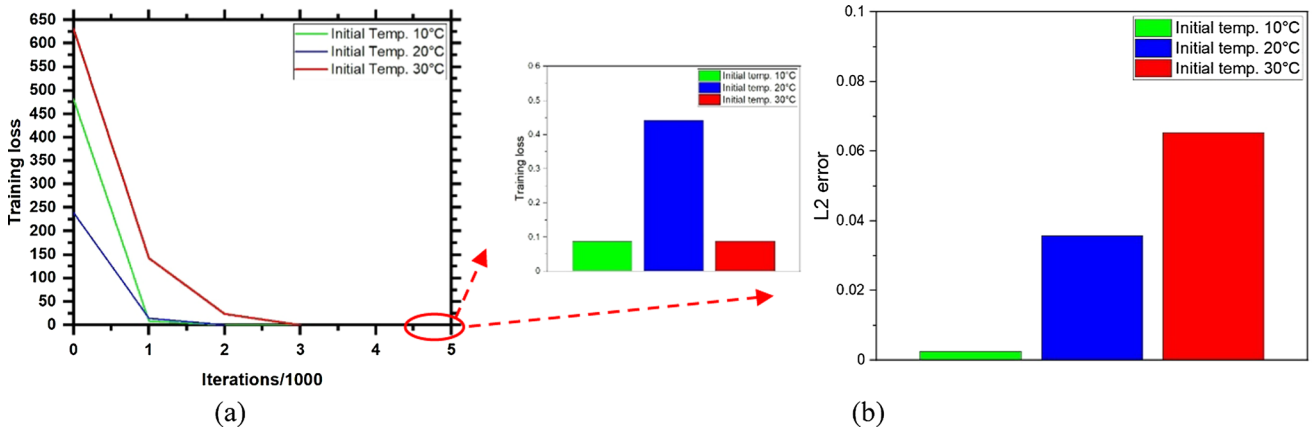

Fig. 8 Cement hydration temperature prediction: **a** training loss and **b** L2 norm of the error vector

20 °C, and 30 °C. The model initiates with an initial loss and progressively reduces this loss with each iteration until it reaches a minimum value as shown in Fig. 8a. After 5000 iterations, the training loss diminishes to 0.0873, 0.4415, and 0.0884 for initial curing temperatures of 10 °C, 20 °C, and 30 °C, respectively. This achievement attests to the successful training process of the developed PINN-CHK architecture. The convergence speed and accuracy are assessed by examining the relative L2 norm of the error vector. The L2 error serves as an indicator of the model's performance. In Fig. 8b, the L2 errors measure 0.00255, 0.03579, and 0.06548 in the trained PINN-CHK models for initial curing temperatures of 10 °C, 20 °C, and 30 °C, respectively. This demonstrates a faster convergence rate, characterized by the gradual reduction in relative L2 values during each iteration. Consequently, it ensures efficient computations and higher predictive accuracy.

Figure 9 depicts the data-driven solution to the cement hydration problems for initial curing temperatures of 10 °C, 20 °C, and 30 °C. An initial curing temperature of 10 °C shows a maximum temperature of ∼ 70 °C, an initial curing temperature of 20 °C comes up with a maximum temperature of ∼ 80 °C, and an initial curing temperature of 30 °C comes up with a maximum temperature

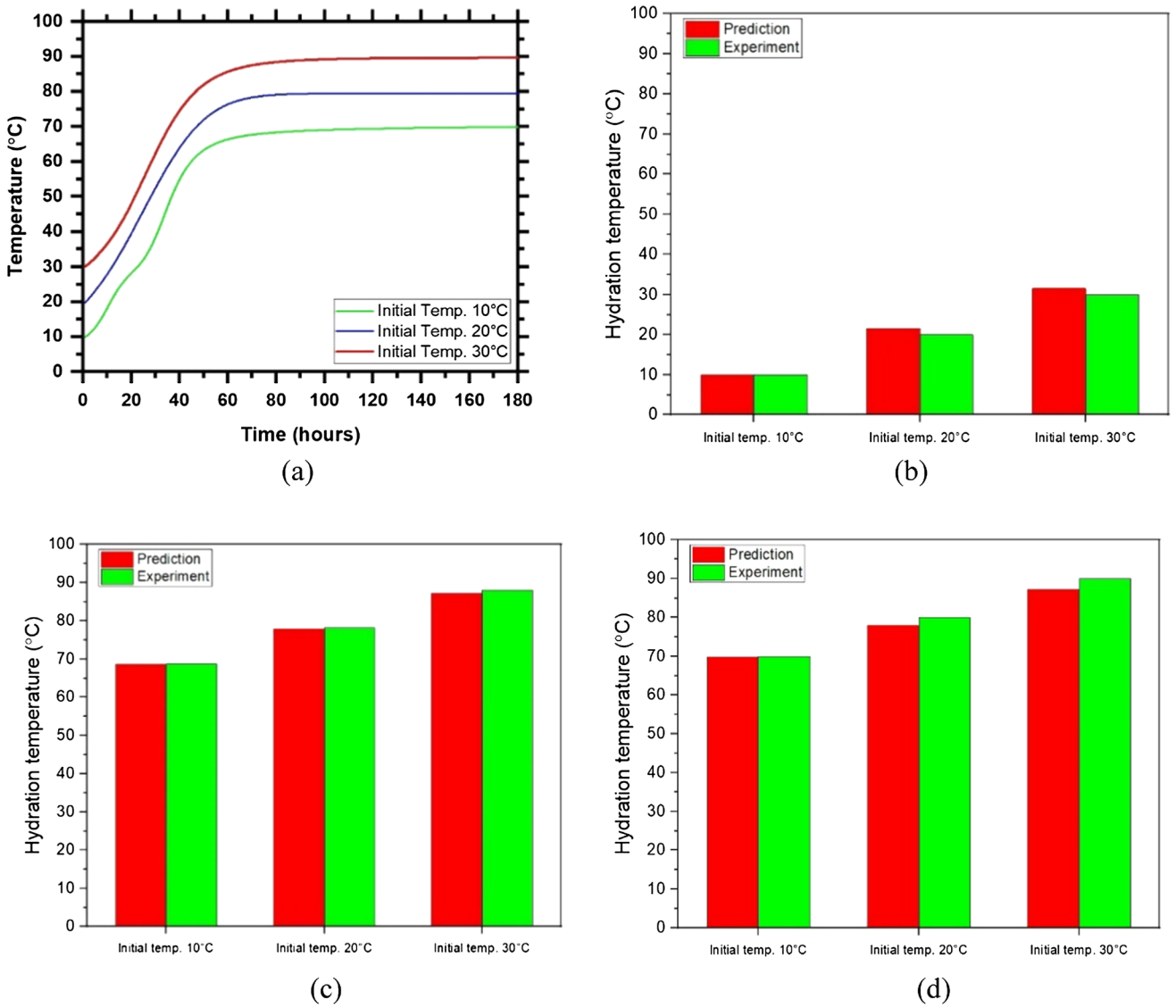

Fig. 9 PINN-CHK predictions on an adiabatic temperature test of ordinary Portland cement: **a** average cement hydration temperature, **b** at time t = 1 h, **c** at time t = 90 h, and **d** at time t = 180 h

of ∼ 90 °C, at the end of 180 h. As depicted in Fig. 9a, the developed PINN-CHK initially assimilates knowledge from the training data and the hydration PDEs for an initial curing temperature of 10 °C. Subsequently, it applies this acquired knowledge to make temperature predictions for other initial curing temperatures, namely 20 °C and 30 °C. These findings align with the experimental data on early-age temperature rise [43, 44]. Upon comparing the predicted temperatures with the experimental data at time points t = 1 h, 90 h, and 180 h, it becomes evident that the results align consistently with the experimental data for different initial and boundary conditions.

The descriptive statistics as shown in Table 5 also finds predictions closely aligning with experimental data across initial curing temperatures of 10 °C, 20 °C, and 30 °C. The minimum, maximum, and mean values of the PINN-CHK model in predicting cement hydration temperatures demonstrate a high level of accuracy and precision. The small standard deviation variations within 2% indicate the model's reliability and consistency in capturing the underlying patterns in the data. This suggests practical applicability, making the model a robust tool for estimating temperatures during the curing process in construction. The fact that the model performs well across a range of initial curing temperatures suggests that it has successfully generalized from the training data to new, unseen conditions. This is a positive sign for the model's applicability to real-world situations with varying curing temperatures.

Thus, the developed PINN-CHK exhibits a close fit to the training data, indicating its proficiency in capturing the

Table 5 Descriptive statistics of the cement hydration temperature

		Temperature (°C)				
	Variable	Min	Max	Mean	Std	Std. (+ / −)
Initial Temp. 10 °C	Experiment	10	70.25	59.68	17.18	–
	Prediction	9.94	69.89	59.48	17.38	1.16%
Initial Temp. 20 °C	Experiment	20	80.50	68.88	17.07	–
	Prediction	19.78	79.50	69.88	17.17	0.59%
Initial Temp. 30 °C	Experiment	30	90.60	78.54	17.13	–
	Prediction	30.14	89.62	79.58	17.32	1.11%

underlying patterns within the dataset. Furthermore, the model's superior generalization performance on unseen physics-informed constraints such as different initial conditions is a key indicator that there is no overfitting. Overall, these characteristics collectively contribute to the assertion that your PINN-CHK model is unbiased and well-suited for real-world applications. However, not properly incorporating external factors, material properties, or environmental conditions may lead to biased model predictions. The PINN-CHK model undergoes training using material properties and parameters outlined in Sect. 2.4.2. Influences like humidity, ambient temperature, and other environmental conditions can affect cement hydration and properties, requiring careful consideration when incorporating them into the model.

Finally, the cement hydration temperature values predicted by PINN-CHK can be employed to determine the evolution of concrete maturity and strength over time. While temperature influences the kinetics of hydration, it may not have a substantial effect on the development of maturity and strength as shown in Fig. 10. Figure 10a shows the concrete maturity which is consistent with the temperature rise pattern as shown in Fig. 9a. Strength increases with the increase in maturity, as shown in Fig. 10b. It is confirmed that concrete with different curing temperatures can reach the ultimate strength (27.4 MPa) within 7 days of curing in this analysis. The phenomenon where cement hydration temperature varies with different initial curing temperatures while maintaining similar maturity and strength profiles can be attributed to the intricate interplay of chemical and physical processes during cement hydration. Cement hydration is highly temperature-dependent, with elevated temperatures accelerating the reaction kinetics, resulting in higher early-age temperature peaks. Nonetheless, even in the presence of temperature fluctuations, if the reference temperature matches the initial curing temperature, and there's initially no temperature gradient, the formation of hydration products can exhibit a consistent pattern, resulting in similar maturity and strength development. This behavior can be understood through the Arrhenius-like temperature dependence of cement hydration kinetics, where increased temperature accelerates the reaction rate. As a result, while the temperature profiles differ, the cumulative effect on

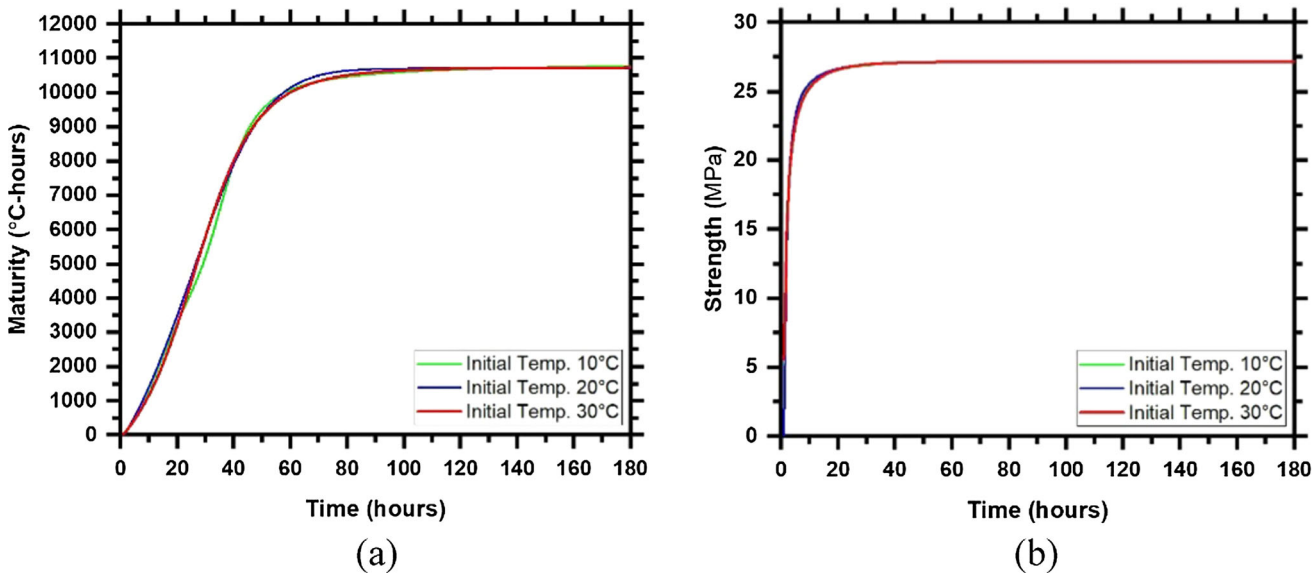

Fig. 10 PINN-CHK predictions: **a** concrete maturity, **b** compressive strength

maturity and strength is similar due to compensatory changes in the reaction rates. This highlights the complex and finely balanced nature of cement hydration, where the interplay of temperature, time, and reaction kinetics ultimately influences material properties.

Thus, by harnessing the capabilities of PINN-CHK, it is possible to effectively reconstruct the intricate cement hydration kinetics, even with a limited volume of training data. The trained network exhibits a high level of reliability, enabling it to confidently generate predictions and extrapolate solutions for various model inputs. Therefore, it excels not only in temperature prediction but also in comprehensively capturing the broader aspects of concrete maturity, strength development, and the fundamental physical phenomena linked to cement hydration kinetics, in contrast to the preceding cement hydration kinetics neural network model [64]. Predicting early-age cement hydration temperature with the PINN-CHK model has significant implications for the construction industry. It optimizes concrete mixtures, facilitating the design of structures with desired properties, strength, and durability. The predictive capability enhances construction scheduling, ensuring quality control and mitigating risks of issues or delays. It contributes to quality control during construction by monitoring and controlling temperatures to prevent issues like cracking. The findings contribute to informed material selection, allowing engineers to tailor concrete compositions for specific real-world applications. Ultimately, the implications extend across improved construction practices, resource utilization, and advancements in the field of cement-based materials. This represents a significant technological advancement and underscores the innovation in PINN model development.

4 Conclusion

This work develops a physics-informed neural network approach for assessing the cement hydration kinetics in fresh cement paste. The technical depth of the developed PINN-CHK model is exemplified by its intricate handling of computational complexity. Integrating physics-informed constraints with neural networks necessitates solving complex PDE-based governing equations of cement hydration while optimizing the neural network concurrently. Achieving scalability involves optimizing the architecture and parallelization strategies to handle increased computational demands and available data efficiently. The success of the developed PINN-CHK model in predicting critical aspects of cement hydration, such as temperature, maturity, and strength, is attributed to its remarkable capacity to reconstruct these intricate processes with limited training data. The network's flexibility and capacity to comprehend complex data patterns empower it to offer precise predictions and extrapolate solutions for diverse inputs within its model.

PINN-CHK accurately captures the temperature development in one-dimensional cement paste domains. The governing equation accounts for time-dependent coupling among the heat transfer, equivalent age, and maturity equations. The neural network is trained with appropriate initial and boundary conditions based on the experimental data, minimizing the loss function. The in-depth analysis provides essential guidance for model selection based on the quantity of training data, shedding light on the nuanced interplay between data, model architecture, and predictive accuracy in the context of cement hydration temperature prediction. The fidelity of the PINN-CHK is determined by three primary hyperparameters: the number of neurons, the number of hidden layers, and the learning rate. Optimal hyperparameter combinations for the PINN-CHK have been determined by considering the trade-off between solution accuracy and computation time. PINN-CHK's success is due to its optimized architecture with three layers of 24 neurons each, operating at a learning rate of 1×10^{-3} and trained on just 5% of the available data. Weight distribution analysis reveals the performance characteristics of individual layers. Statistical metrics, including mean-squared error, reinforce these selections, supporting the training process under specific conditions. Box plots graphically show the numerical spread of the PINN-CHK prediction errors through the quartiles. PINN-CHK predicts the temperature rise during cement hydration in OPC400 specimens under adiabatic conditions. For instance, with an initial curing temperature of 10 °C, 20 °C, and 30 °C the trained PINN-CHK predicts a hydration temperature of approximately 70 °C, 80 °C, and 90 °C at the end of 180 h. Notably, the PINN-CHK model predictions yield satisfactory results, with absolute differences as low as 0.5–3.5 °C when compared to experimental findings. This validation demonstrates the effectiveness of this physics-informed model.

PINN-CHK leverages automatic differentiation for mesh-free modeling which improves the convergence rate, offering a data-driven alternative to finite element methods. What stands out as particularly noteworthy is the comprehensive analysis of accuracy, generalization, and susceptibility, which extends beyond statistical comparisons to encompass considerations of overfitting and underfitting. PINN-CHK shines as a more appropriate choice when data is limited. It outperforms conventional machine learning methods by satisfying both data and governing equations of the cement hydration kinetics. Conventional neural network architectures may struggle in predicting early-age cement hydration temperature due to their limited ability to explicitly enforce physics-based constraints. In contrast,

the unique design of PINN-CHK architecture excels in integrating domain knowledge, ensuring accurate and physically meaningful predictions of early-age cement hydration. By seamlessly complementing laboratory experiments and underlying physics, PINN-CHK enhances the depth and breadth of knowledge surrounding cement hydration kinetics. This comprehensive understanding helps mitigate thermal cracking risks, informs material selection for concrete mixes, and contributes to environmental sustainability in the construction industry through reduced energy consumption. The incorporation of PINN-CHK as a physics-guided approach marks a significant potential shift in industry practices related to cement-based materials. This not only enhances the accuracy of predictions but also showcases the potential of hybrid models that blend domain-specific knowledge with data-driven techniques.

In summary, PINN-CHK is designed to capture the early-age cement hydration temperature, concrete maturity, and strength in cement-based materials, presenting a novel and high-fidelity prediction approach to representing cement hydration phenomena across different spatial and temporal scales. The novelty of this work lies in embedding the cement hydration physics into the loss function to produce results from any inputs. PINN-CHK excels in generalization, especially when confronted with minimal training data, possibly due to this physics-informed nature. This sets the stage for improving model accuracy by incorporating multi-physics coupling, leveraging data-driven approaches, and enhancing generalization capabilities. Real-time monitoring, collaboration between computational and experimental studies, and exploring novel cement-based materials or sustainable alternatives represent promising directions for further advancements. Overall, PINN-CHK offers valuable insights for optimizing concrete curing, promoting resource efficiency and potentially reducing associated costs. This knowledge will aid in assessing the long-term performance of structures and drive ongoing research and development, fostering innovations in cement-concrete formulations and AI-based construction methodologies. The ethical use of AI in construction revolves around ensuring transparency, fairness, accountability for errors, regulatory compliance, worker impact, and data security. PINN-CHK paves the way for making AI models more interpretable, mitigating biases in training data, establishing clear accountability mechanisms for errors, and complying with industry regulations.

Author contributions The authors confirm their contribution to the paper as follows: Md. Asif Rahman, Yang Lu did study conception and design; Md Asif Rahman developed the model, done programming, analysis and data collection and drafted manuscript preparation; Yang Lu and Tianjie Zhang drafted the manuscript review; Yang Lu approved the final version manuscript.

Funding This research received no specific grant from funding agencies in the public, commercial, or not-for-profit sectors.

Data availability Data will be made available upon reasonable request and nondisclosure agreement.

Code availability The code is being updated. The pseudo-code can be found in the GitHub repository (https://github.com/mdasifrahman108/Cement_Hydration_Temperature).

Declarations

Conflict of interest The authors declare that they have no known competing financial interests or personal relationships that could have appeared to influence the work reported in this paper.

Consent for publication Not applicable.

Ethical approval Not applicable.

References

1. Wang XY, Lee HS (2010) Modeling the hydration of concrete incorporating fly ash or slag. Cement Concrete Res 40(7):984–996. https://doi.org/10.1016/j.cemconres.2010.03.001
2. Waller V, d'Aloïa L, Cussigh F, Lecrux S (2004) Using the maturity method in concrete cracking control at early ages. Cement Concrete Compos 26(5):589–599
3. Kunther W, Dai Z, Skibsted J (2016) Thermodynamic modeling of hydrated white Portland cement–metakaolin–limestone blends utilizing hydration kinetics from 29Si MAS NMR spectroscopy. Cement Concrete Res 86:29–41. https://doi.org/10.1016/j.cemconres.2016.04.012
4. Safiuddin M, Kaish AA, Woon CO, Raman SN (2018) Early-age cracking in concrete: causes, consequences, remedial measures, and recommendations. Appl Sci 8(10):1730
5. ACI Committee 207, Mass concrete. American Concrete Institute, USA Committee Report ACI 207.1R-96, 1996.
6. Almusallam AA (2001) Effect of environmental conditions on the properties of fresh and hardened concrete. Cement Concr Compos 23(4–5):353–361
7. Neville AM (2000) Propriétés des bétons. Eyrolles, Paris
8. Junior AN, Ferreira SR, Toledo Filho RD, Fairbairn EDMR, Dweck J (2019) Effect of early age curing carbonation on the mechanical properties and durability of high initial strength

Portland cement and lime-pozolan composites reinforced with long sisal fibres. Compos Part B: Eng 163:351–362
9. Davie CT, Pearce CJ, Bićanić N (2006) Coupled heat and moisture transport in concrete at elevated temperatures—Effects of capillary pressure and adsorbed water. Num Heat Trans, Part A: Appl: Int J Comput Methodol 49(8):733–763
10. Bentz DP (2008) A review of early-age properties of cement-based materials. Cem Concr Res 38:196–204
11. Nehdi M, Soliman A (2011) Early-age properties of concrete: overview of fundamental concepts and state-of-the art research. Proc Inst Civ Eng Constr Mater 164:57–77
12. Mihashi H, Leite JPDB (2004) State-of-the-art report on control of cracking in early age concrete. J Adv Concr Technol 2:141–154
13. Klemczak B, Knoppik-Wróbel A (2011) Early age thermal and shrinkage cracks in concrete structures-description of the problem. Archit-Civ Eng-Environ 4:35–48
14. Holt EE (2001) Early Age Autogenous Shrinkage of Concrete. Espoo, Finland, Technical Research Centre of Finland
15. Holt E, Leivo M (2004) Cracking Risks Associated with Early Age Shrinkage. Cem Conc Compos 26:521–530
16. ACI Committee 224 (2007). Causes, Evaluation, and Repair of Cracks in Concrete Structures; American Concrete Institute: Farmington Hills, MI, USA
17. Jennings HM, Johnson SK (1986) Simulation of microstructure development during the hydration of a cement compound. J Am Ceram Soc 69:790–795
18. Pommersheim JM, Clifton JR (1979) Mathematical modeling of tricalcium silicate hydration. Cem Concr Res 9:765–770
19. F Tomosawa, (1997) Development of a Kinetic Model for Hydration of Cement, in: H. Justnes (Ed.). In: Proceedings of the Tenth International Congress on the Chemistry of Cement, Göteburg, Sweden, 1997, p. 2ii051.
20. Lothenbach B, Winnefeld F (2006) Thermodynamic modelling of the hydration of Portland cement. Cem Concr Res 36:209–226
21. F Tomosawa, T Noguchi, C Hyeon, (1997) Simulation model for temperature rise and evolution of thermal stress in concrete based on kinetic hydration model of cement, in: S. Chandra (Ed.). In: Proceedings of Tenth International Congress Chemistry of Cement. Gothenburg, Sweden, 4: 72–75.
22. Park K-B, Jee N-Y, Yoon I-S, Lee H-S (2008) Prediction of temperature distribution in high-strength concrete using hydration model. ACI Mater J 105:180–186
23. Swaddiwudhipong S, Shen D, Zhang MH (2002) Simulation of the exothermic hydration process of Portland cement. Adv Cem Res 14:61–69
24. Cook R, Han T, Childers A, Ryckman C, Khayat K, Ma H, Kumar A (2021) Machine learning for high-fidelity prediction of cement hydration kinetics in blended systems. Mater Des 208:109920
25. Jambunathan K, Hartle S, Ashforth-Frost S, Fontama V (1996) Evaluating convective heat transfer coefficients using neural networks. Int J Heat Mass Transfer 39(11):2329–2332
26. Liu Y, Dinh N, Sato Y, Niceno B (2018) Data-driven modeling for boiling heat transfer: using deep neural networks and high-fidelity simulation results. Appl Therm Eng 144:305–320
27. Kim J, Lee C (2020) Prediction of turbulent heat transfer using convolutional neural networks. J Fluid Mech 882:A18
28. Fonda E, Pandey A, Schumacher J, Sreenivasan KR (2019) Deep learning in turbulent convection networks. Proc Natl Acad Sci 116(18):8667–8672
29. Smith R, Dutta S (2021) Conjugate thermal optimization with unsupervised machine learning. ASME J Heat Transfer 143(5):052901
30. Beintema G, Corbetta A, Biferale L, Toschi F (2020) Controlling Rayleigh-Benard convection via reinforcement learning. J Turbul 21(9–10):585–605
31. Hachem E, Ghraieb H, Viquerat J, Larcher A, Meliga P (2020). Deep reinforcement learning for the control of conjugate heat transfer with application to workpiece cooling. arXiv preprint arXiv:2011.15035.
32. Hu Q, Zhao Y, Wang Y, Peng P, Ren L (2023) Remaining useful life estimation in prognostics using deep reinforcement learning. IEEE Access 11:32919–32934
33. Li X, Ding Q, Sun JQ (2018) Remaining useful life estimation in prognostics using deep convolution neural networks. Reliab Eng Syst Saf 172:1–11
34. Xia M, Zheng X, Imran M, Shoaib M (2020) Data-driven prognosis method using hybrid deep recurrent neural network. Appl Soft Comput 93:106351
35. Namdari A, Samani MA, Durrani TS (2022) Lithium-ion battery prognostics through reinforcement learning based on entropy measures. Algorithms 15(11):393
36. Raissi M, Perdikaris P, Karniadakis GE (2019) Physics-informed neural networks: a deep learning framework for solving forward and inverse problems involving nonlinear partial differential equations. J Comput Phys 378:686–707. https://doi.org/10.1016/j.jcp.2018.10.045
37. Hennigh O, Narasimhan S, Nabian MA, Subramaniam A, Tangsali K, Rietmann M, Ferrandis JDA, Byeon W, Fang Z, and Choudhry S (2021). NVIDIA SimNet^{TM}: An AI-accelerated multi-physics simulation framework. In: International conference on computational science (pp. 447-461). Cham: Springer International Publishing.
38. Cai S, Wang Z, Chryssostomidis C, Karniadakis GE (2020). Heat transfer prediction with unknown thermal boundary conditions using physics-informed neural networks. In: Fluids Engineering Division Summer Meeting (Vol. 83730, p. V003T05A054). American Society of Mechanical Engineers.
39. Wang T, Huang Z, Sun Z, Xi G (2021) Reconstruction of natural convection within an enclosure using deep neural network. Int J Heat Mass Transfer 164:120626
40. Cai S, Wang Z, Fuest F, Jeon YJ, Gray C, Karniadakis GE (2021) Flow over an espresso cup: inferring 3-D velocity and pressure fields from tomographic background oriented Schlieren via physics-informed neural networks. J Fluid Mech 915:A102
41. Ye Y, Fan H, Li Y, Liu X, Zhang H (2022) Deep neural network methods for solving forward and inverse problems of time fractional diffusion equations with conformable derivative. Neurocomputing 509:177–192. https://doi.org/10.1016/j.neucom.2022.08.030
42. Lu Lu, Xuhui Meng, Zhiping Mao, George E. Karniadakis, DeepXDE: A deep learning library for solving differential equations, arXiv:1907.04502.
43. Koichi Maekawa, Rajesh Chaube, Toshiharu Kishi, (1998) Modeling of Concrete Performance: Hydration, Microstructure Formation and Mass Transport, ROUTLEDGE, London
44. Maekawa K, Ishida T, Kishi T (2009) Multi-scale Modeling of Structural Concrete. Taylor & Francis, London
45. Vagelis G (1999) Papadakis, Experimental investigation and theoretical modeling of silica fume activity in concrete. Cem Concr Res 29:79–86
46. Vagelis G, Papadakis S (2000) Tsimas, Effect of supplementary cementing materials on concrete resistance against carbonation and chloride ingress. Cem Concr Res 30:291–299
47. Papadakis VG (1999) Effect of fly ash on Portland cement systems: Part I. Low-calcium fly ash. Cement Concrete Res 29(11):1727–1736
48. Papadakis VG (2000) Effect of fly ash on Portland cement systems, Part II: high calcium fly ash. Cem Concr Res 30:1647–1654

49. Papadakis VG, Vayenas CG, Fardis MN (1991) Physical and chemical characteristics affecting the durability of concrete. ACI Mater J 88:186–196
50. Saeki T, Monteiro PJM (2005) A model to predict the amount of calcium hydroxide in concrete containing mineral admixture. Cem Concr Res 35:1914–1921
51. Pane I, Hansen W (2005) Investigation of blended cement hydration by isothermal calorimetry and thermal analysis. Cem Concr Res 35:1155–1164
52. Hernandez-Bautista E, Bentz DP, Sandoval-Torres S, Cano-Barrita J (2014) modeling heat and moisture transport during hydration of cement - based materials in semi - adiabatic conditions. Cement Concr Compos 69:38–48
53. Laplante P, Roussel S, Lecrux S (1998). Maturity-measurement technique: the Arrhenius law in the service of construction sites. In: Concrete, from material to structure. International RILEM Conference, Arles, France (pp. 323-42).
54. Chini AR, Acquaye L (2005) Effect of elevated curing temperatures on the strength and durability of concrete. Mater Struct 38:673–679
55. Mills RH (1966) Factors influencing cessation of hydration in water cured cement pastes. Highway Res Board Spec Rep 90:406–424
56. Mukhopadhyay AK, Ye D, Zollinger DC (2006). Moisture-related cracking effects on hydrating concrete pavement (Vol. 7). College State, TX, USA: Texas Transportation Institute, Texas AM University System.
57. Saul AGA (1951) Principles underlying the steam curing of concrete at atmospheric pressure. Mag Concr Res 2(6):127
58. Kee CF (1971) Relation between strength and maturity of concrete. Proc ACI J 68(3):196–203
59. Paszke A, Sam G, Chintala S, Chanan G, Yang E, DeVito Z, Lin Z, Desmaison A, Antiga L, and Lerer A. (2017) Automatic differentiation in pytorch. https://openreview.net/forum?id=BJJsrmfCZ.
60. Glorot X, Bengio Y (2010) Understanding the difficulty of training deep feedforward neural networks. J Mach Learn 9:249–256
61. Griewank A et al (1989) On automatic differentiation. Math Programm: Recent Develop Appl 6(6):83–107
62. Liu DC, Nocedal J (1989) On the limited memory BFGS method for large scale optimization. Math Program 45:503–528
63. MD Zeiler, Adadelta: An adaptive learning rate method, arXiv: 1212.5701.
64. Wang L, Yang B, Chen Y, Zhao X, Chang J, Wang H (2012) Modeling early-age hydration kinetics of Portland cement using flexible neural tree. Neural Comput Appl 21:877–889